

**REVIEW OF AERONAUTICAL FATIGUE
INVESTIGATIONS IN JAPAN
DURING THE PERIOD JUNE 2011 TO MAY 2013**

Edited by

Nobuo Takeda
The University of Tokyo

Shigeru Machida
JAXA

For Presentation at the 33rd Conference of
the International Committee on Aeronautical Fatigue and Structural Integrity

Jerusalem Israel, 3-4 June, 2013

Contents

	page
1. INTRODUCTION	4
2. FATIGUE AND FAILURE IN METALLIC MATERIALS AND COMPONENTS	5
2.1 Fatigue Notch Factor for Aerospace Materials Based on Weakest Link Failure Theory and the Critical Distance	5
2.2 New Monitoring Method for Mechanical Joint Using Structural Damping Properties	6
2.3 Property for Fatigue Crack Propagation of Friction Stir Welded 2024-T3 Aluminum alloy	9
2.4 Evaluation of Pre-Corrosion Damage on Fatigue Behavior of Friction Stir Welded 2024-T3 Aluminum Alloy	10
2.5 Research and Development of CMOS-inverter Oscillator Circuit Strain Measurement System	11
3. FATIGUE AND FAILURE IN METAL/COMPOSITE HYBRID MATERIALS	13
3.1 Bearing Behavior of Bolted Joints in Thin Titanium Films / CFRP Hybrid Laminate	13
3.2 Effects of Transition Region Structure on Mechanical Behavior of Thin Titanium Films / CFRP Hybrid Laminate	14
4. FATIGUE AND FAILURE IN COMPOSITE MATERIALS AND COMPONENTS	16
4.1 Suppression of Delamination Crack for the Foam Core Sandwich Panel Joint	16
4.2 Electric Characteristic Analysis of Composite Structure by Lightning Strike	17
4.3 Optical Measurement of Spark Phenomena on CFRP Specimens with Fasteners by Lightning Strike	18
4.4 Evaluation of Notched Strength and Damage Behaviour in Non-crimp Fabric Based Composites	18

4.5 Effect of Fiber Volume Fraction on First Transverse Crack Formation in Cross-Ply CFRP Laminates under Fatigue Loading	20
4.6 Durability Evaluation of Carbon/BMI Composites after Thermal Aging (DECATA)	21
4.7 Application of Bayesian Analysis to Determining Fatigue Load on Composite Structures	24
5. STRUCTURAL HEALTH MONITORING	25
5.1 Hierarchical Fiber-optic System for Detecting Impact Damage in Large-scale Composite Structure	25
5.2 Development Status of Structural Health Monitoring Technologies Using Optical Fiber Sensors at MHI	28
6. FULL-SCALE TESTING	30
6.1 XP-1/XC-2 Full Scale Strength Test	30
6.2 Manufacturing Demonstration of a Prepreg - VaRTM Hybrid Composite Aircraft Part and Its Evaluation	31
ACKNOWLEDGEMENTS	32
TABLES AND FIGURES	33

1. INTRODUCTION

Nobuo Takeda, National Delegate, The University of Tokyo

This review summarizes the papers on the study of aeronautical fatigue, structural integrity and related themes conducted in Japan during June 2011 to May 2013.

The papers were contributed by following organizations:

Japan Aerospace Exploration Agency (JAXA)
 Technical Research and Development Institute (TRDI), MOD
 Mitsubishi Heavy Industries, Ltd. (MHI)
 Kawasaki Heavy Industries, Ltd. (KHI)
 Fuji Heavy Industries, Ltd. (FHI)
 IHI Corporations
 The University of Tokyo
 Tokyo University of Science
 Waseda University
 Nagoya University

The general activities on aircraft development program in Japan during 2011 to 2013 is summarized as follows:

- The development of MRJ (Mitsubishi Regional Jet, 70- to 90-seat regional jets) aircraft is underway. The production started at Mitsubishi Aircraft Corporation in Nagoya. The maiden flight is expected late in 2013.
- Both XP-1, the 4 turbo-fan mid-size maritime patrol airplane and XC-2, the twin turbo-fan large-size cargo transport airplane, have been subject to the final tests including full-scale static test and full scale fatigue test. Both XP-1 and XC-2 made the first flight in September, 2007 and in January, 2010, respectively.
- “Civil Aviation Fundamental Technology Program -Advanced Materials & Process Development for Next-Generation Aircraft Structures” (FY2008-2012) have been conducted at the Materials Process Technology Center, in collaboration with industries, universities and national laboratories. The program includes two projects on (1) Composite Structure Health Monitoring and Diagnosis, and (2) Material Development and Processing of Next-Generation Titanium Alloy Structural Members.

2. FATIGUE IN METALLIC MATERIALS AND COMPONENTS

2.1 Fatigue Notch Factor for Aerospace Materials Based on Weakest Link Failure Theory and the Critical Distance

Youichi Yamashita, Yusuke Ueda and Hiroshi Kuroki
IHI Corporation, Tokyo, Japan;

Foreign object damage (FOD) often causes small notches on leading edge of airfoil (Fig. 1). The method for estimating the fatigue strength of small-notched specimens of aerospace materials were investigated [1-3] using the Theory of Critical Distance (TCD). The TCD employs the stress distribution in the vicinity of the notch. In Ti alloy Ti-6Al-4V, the calibrated critical distances have an almost constant value [1, 2]. In Ni base super-alloy In718, the longer fatigue life gives the smaller critical distance [3]. It has been found that a good correlation exists between the critical distance stress (average stress within the critical distance) and crack initiation life if the critical distance is calibrated by the two notched fatigue failure curves of different notch root radii (Fig.1) [3].

This study investigated fatigue notch factors for small-notched aerospace materials based on the weakest link failure theory using the TCD. Figure 2 shows the schematic of the difference in fracture process zone (FPZ) between smooth specimen and notch specimen. The round-bar smooth specimen can have a much larger FPZ, V_{smooth} , than the circumferential notched specimen. The fatigue fracture process zone, V_{notch} , of the circumferential notch specimen is limited in the vicinity of the notch tip.

Fatigue notch factor can be determined with the stress concentration factor within critical distance region and the volume ratio of FPZ in notch specimen to that of smooth specimen for a failure cycles as the following:

$$K_f = \frac{\sigma_{smooth}}{\sigma_{notch}} = \left(\frac{V_{notch}}{V_{smooth}} \right)^{1/m} \cdot \frac{\sigma_{CD}}{\sigma_{notch}} \quad (1)$$

In Eq. (1), $(V_{notch}/V_{smooth})^{1/m}$ means the volume effects between notch and smooth specimens with the $1/m$ power where m is the shape parameter of the two-parameter Weibull distribution and $\sigma_{CD}/\sigma_{notch}$ means the average stress concentration factor in FPZ of notch specimen. The critical distance stress, σ_{CD} , and fatigue notch factor, K_f , can be simply approximated as the following:

$$\sigma_{CD} = \frac{\int_0^{L_1} \sigma_{yy}(r) dx}{L_1} = \frac{K_t}{2\sqrt{2}L_1} \left[2\rho^{\frac{1}{2}} \left(L_1 + \frac{\rho}{2} \right)^{\frac{1}{2}} - \rho^{\frac{3}{2}} \left(L_1 + \frac{\rho}{2} \right)^{\frac{-1}{2}} \right] \sigma_{notch} \quad (2)$$

$$K_f = \frac{\sigma_{smooth}}{\sigma_{notch}} = \frac{K_t}{2\sqrt{2}L_1} \left[2\rho^{\frac{1}{2}} \left(L_1 + \frac{\rho}{2} \right)^{\frac{1}{2}} - \rho^{\frac{3}{2}} \left(L_1 + \frac{\rho}{2} \right)^{\frac{-1}{2}} \right] \left(\frac{V_{notch}}{V_{smooth}} \right)^{1/m} \quad (3)$$

Here, the Glinka's closed-form stress distribution (Eq. (4)) at notch root region has been used.

$$\sigma_{yy}(r) = \frac{K_t}{2\sqrt{2}} \left[\left(\frac{\rho}{r} \right)^{\frac{1}{2}} + \frac{1}{2} \left(\frac{\rho}{r} \right)^{\frac{3}{2}} \right] \sigma_{notch} \quad (4)$$

In Eq. (4), x and r have the relation of $x = r + \rho/2$. K_t is stress concentration factor of the small notch tip. Figure 3 depicts the non-dimensional fatigue strength of both materials with various notch depths at 10^7 cycles fatigue failure life. Fatigue notch factors of small notched specimens can be well predicted.

References

- [1] Yamashita Y., Ueda Y., Kuroki H. and Shinozaki M. (2009), Proc of ICAF 2009.
- [2] Yamashita Y., Ueda Y., Kuroki H. and Shinozaki M. (2010), Eng Fract Mech, 77, 1439–1453.
- [3] Yamashita Y., Ueda Y., and Kuroki H. (2009), Proc of ICAF 2011.

2.2 New Monitoring Method for Mechanical Joint Using Structural Damping Properties

Shigeru Machida¹, Shuji Kishishita², Yuya Ito³, Takao Okada¹, Motoo Asakawa³

¹Japan Aerospace Exploration Agency (JAXA), Tokyo, Japan

²Advanced Engineering Services, Tsukuba, Japan

³Waseda University, Tokyo, Japan

The term of ‘‘Structural Damping’’ means the energy dissipation properties of structure. It is well known that interfacial slip phenomena at structural joint has a significant role to determine structural damping which affected by type of joint and conditions of faying surfaces. From fatigue evaluation point of view, faying surfaces of mechanical joints have a tendency of degradation during cyclic loading,

such as fretting wear, corrosion and cracking and it is easy to understand that such degradation can change the structural damping capability.

In order to qualify the relationship between dissipation energy of structural joint and condition of faying surfaces, rivet joint specimens were tested under constant cyclic loading. Specimens can represent the part of circumferential single lap joint which has typical three rivet rows. 2024-T3 clad sheet, thickness $t=1.27\text{mm}$, was used for both inner and outer skins and NAS1097AD5 countersunk rivets were installed with a row pitch of 20mm (Fig. 4). The tests were conducted under load control using a constant amplitude sinusoidal waveform at a frequency of 3Hz. The stress applied to the specimens was 83.5Mpa at $R=0.1$ assumed to be the same level as hoop stress of fuselage skin under cabin pressure condition. The total number of cycles on each specimen was varied from 1,000 to 180,000 to investigate faying surface condition at each cycle. Stopping cyclic loading at specific cycles, an extensometer was installed at the side edge of specimen to measure deflection between two points over the rivet joint, gage length 140mm and cyclic loading was applied at a frequency of 1Hz for measuring dynamic force and displacement. After the completion of total number of cycle, removing all rivets carefully and faying surfaces of all specimens were inspected. The test results show the unique relationship between Energy Dissipation D and number of cycles qualitatively (Fig. 5).

Initial Phase;

At very early stage of load cycling, 0-300cycles, D values are scattered within the range of $200 \times 10^{-6}\text{J}$ which caused by manufacturing and riveting process, such as manufacturing tolerance of holes and squeeze force.

Fretting Phase 1;

In the phase of lower number of cycles less than 10,000, D values are decreasing. In this phase, metal-to-metal contact phenomena affects behavior of D values mainly.

Fretting Phase 2;

In the range of 10,000 to 30,000 cycles, D values exhibit plateau behaviour. The results indicate that energy dissipation by the wear process during cyclic loading is dominant over growth of metal-to-metal contacts.

Fretting Phase 3;

Beyond 30,000 cycles, severe fretting wears are observed around many rivet holes. It is clear that wear debris moves and sticks again during cycles. It is the phase of forming severe fretting wears before creating crack damage.

For characterizing degradation and damages inside a mechanical joint from the information of structural damping quantitatively, an analytical joint model is established. Metherell and Diller¹⁾ investigated dissipation energy of single lap joint. Their work gives equations which can express a shape of load-deflection hysteresis loop and energy dissipation per cycle under uniform clamping pressure on single lap joint. In order to establish governing equations for single lap joint with rivets which has stick part and slip part to transfer loads, the stiffness of stick portion, K_{ST} , is introduced. It is assumed as the model of Metherell and Diller that the length of slip portion is proportional to tensile load in the skins and shear force per unit length on slip portion is expressed as the product of width of joint, friction coefficient and uniform clamping pressure. The new equations for the displacement as the function of tensile load are established for rivet joint.

Using data of the load-deflection hysteresis loops from cyclic loading tests, unknown coefficients of the new analysis model are identified. As the results, it is found that this model can express load-deflection hysteresis loops very well and be used for characterizing rivet joint properties.

The following conclusions can be drawn from present study.

- (1) It is experimentally observed the unique relationship between structural damping and number of loading cycles.
- (2) Structural damping can explain the condition of faying surfaces of riveted shear lap joint.
- (3) By using the proposed mathematical joint model, it is possible to quantify the non-linearity of force/displacement hysteresis loop and to identify the coefficients which can explain condition on the faying surface of shear lap joint.
- (4) The analyses suggest that the fretting process is asymmetry during loading and unloading phase. However, more detailed work is necessary to understand the mechanism of the asymmetry of fretting process.

Reference

- 1) A. F. Metherell, S. V. Diller, Instantaneous Energy Dissipation Rate in a lap Joint – Uniform Clamping Pressure, J. Appl. Mech., Vol. 35, 1968, pp. 123-128

2.3 Property for Fatigue Crack Propagation of Friction Stir Welded 2024-T3 Aluminum Alloy

Takao Okada¹, Motoo Asakawa², Toshiya Nakamura¹ and Shigeru Machida¹

¹ Japan Aerospace Exploration Agency (JAXA), Tokyo, Japan

² Waseda University, Tokyo, Japan;

Friction Stir Welding (FSW) has been applied in many industries. Compared to the riveted joint which is common to the aircraft primary structure, production by the FSW could reduce time to fabricate it and its cost. Many properties concerning to the FSW joint have to be evaluated in order to use FSW to the aircraft primary structure.

We have been evaluated fatigue crack growth behavior of the friction stir welded 2024-T3 aluminum alloy for constant amplitude loading condition ($\Delta\sigma=50\text{MPa}$) at $R=0.1$ [1]. Here we present the result of the fatigue crack growth test of FSW panel at different stress amplitude, $\Delta\sigma = 75, 50$ and 25MPa at $R=0.1$. In this study maximum and minimum residual stress caused by the FSW are 186MPa and -10MPa , respectively. Figure 6 shows the fatigue crack growth rate at middle and higher stress range. Same as the previous experience ($\Delta\sigma=50\text{MPa}$), the crack growth rate on FSW panel is accelerated when the crack tip is within and past the weld line. After the crack tip is away from the weld line, crack growth rate of FSW panel close to that of base material. For both stress amplitude, the retardation of crack growth rate is not observed throughout the fatigue test. The test result of $\Delta\sigma = 25\text{MPa}$ is shown in Fig. 7. From the figure, it is observed that the crack propagation rate is decelerated by the compressive residual stress when the crack tip is located before the weld line. After the crack tip reaches the weld line, the crack propagation rate is accelerated by the tensile residual stress.

Next, the maximum ratio between crack growth rate on FSW panel and that on base material are compared for each test condition. The ratio for $\Delta\sigma = 75, 50$ and 25 are $2.1, 2.3$ and 3.7 , respectively. Because all FSW panel using in this study is made under the same FSW condition, residual stress of all specimens considered as identical. It indicates that the lower the stress amplitude, the effect of residual stress is more prominent.

Reference

[1] T. Okada, et. al., "Properties of fatigue crack propagation in friction stir welded 2024-T3 aluminum alloy", Proceedings of the ICAF2009, pp. 899-908.

2.4 Evaluation of Pre-Corrosion Damage on Fatigue Behavior of Friction Stir Welded 2024-T3 Aluminum Alloy

Takao Okada¹, Motoo Asakawa², Toshiya Nakamura¹ and Shigeru Machida¹

¹ Japan Aerospace Exploration Agency (JAXA), Tokyo, Japan

² Waseda University, Tokyo, Japan

Friction Stir Welding (FSW) is capable of welding high strength aluminum alloys and its application has started in many industries. Compared to the riveted joint which is common to the aircraft primary structure, production by the FSW could reduce time to fabricate it and its cost. Many properties concerning to the FSW joint including corrosion resistance have to be evaluated in order to use FSW to the aircraft primary structure. Corrosion behavior on the section perpendicular to the FSW direction is evaluated in Ref. 1. However, exposed surface of the FSW panel is also to be a candidate of corrosion damage and its corrosion resistance needs to be evaluated. In addition, effect of corrosion damage on the fatigue behavior of the FSW joint has to be well understood [2].

Here we present the corrosion test result of the friction stir welded 2024-T3 aluminum alloy. The surface of the joint and the section perpendicular to the weld line are exposed to the 3.0% NaCl solution at room temperature for 24, 48, 72 and 96 hours. The corrosion resistance of the bare 2024-T3 aluminum alloy with same surface finish is also evaluated.

Figure 8(a) shows the corroded surface of the FSW specimen which is exposed 96 hours. This figure shows that the region around weld edge and its center have corrosion pits of which depth are about than 120 μm . The thermo-mechanical affected zone seems to be highly attacked by the corrosion medium. The corroded surface of the base material has the smaller corrosion pits which spread randomly as shown in Fig. 8(b). The depth of the corrosion pits those become fracture origins are about 80 μm and then those depths are also shallower than that of the FSW specimens.

Next, the fatigue test of the pre-corroded FSW specimen and base material is conducted in order to evaluate the effect of corrosion damage on the fatigue life. Result of benign FSW specimen is also shown. Fatigue test result (Fig. 9) indicates that the fatigue life of the base material is a little shorter than that of the FSW specimens. And the fatigue life of the non-corroded FSW specimen is more than 10 times larger than that of the corroded specimen. Then the corrosion

damage has the detrimental effect to the fatigue life. In actual usage, the base material is usually used as clad material. On the other hand, FSW specimen seems to be without clad layer, because of the welding process. So fatigue test of the Al clad 2024-T3 specimen are also conducted and its results are also shown in this figure. The fatigue life of the clad specimen is shorter than that of the non-corroded FSW specimen, because the clad layer becomes fracture origin. And it shows that the fatigue life of the pre-corroded FSW specimen is shorter than that of the Al clad specimen in case the exposure duration is longer. This means that without corrosion damage, FSW specimen with adequate surface finish will have better fatigue performance than the clad base material. However after some amount of corrosion damage exists, its fatigue life reduces drastically.

Based on the test result, it is considered that the FSW joint might be more sensitive to corrosion than the base material and then additional care might be necessary for usage. Currently additional fatigue test is conducted to obtain more fatigue data.

References

- [1] X. Yun, et. al., "Corrosion Behavior during Cyclic Salt Spray Test of Friction Stir Welded A7075 and A6N01 Aluminum Alloys", J. Japan Inst. Metals, Vol. 70, No. 1, 2006, pp. 96-105.
- [2] T. Ghidini, et. al., "Predicting the fatigue life of pristine and pre-corroded friction stir welded joints", Int. J. Structural Integrity, vol. 2, Iss.2, pp. 200-213.

2.5 Research and Development of CMOS-inverter Oscillator Circuit Strain Measurement System

Atsushi Kanda¹, Atsushi Saitoh² and Takao Utsunomiya²

¹ Japan Aerospace Exploration Agency (JAXA)

² Shibaura Institute of Technology

New strain measurement sensor has been developed, which involves a CMOS inverter oscillator circuit instead of a conventional Wheatstone bridge circuit. The new sensor could omit amplifier and become compact because a counting device measures frequency changes of circuit voltage output caused by resistance changes

of a strain gauge. Sensor characteristics were confirmed by static tensile tests of aluminum specimens. The test results showed that accuracy was not enough. However, the same level of accuracy as conventional sensor has been achieved by using simple compensation factor assuming of existence of internal resistance.

For strain measurements, common measurement system employ the Wheatstone bridge circuits and require amplifiers for amplifying the minute voltage changes occurred by the amount of change in the electrical resistance. The new system uses “CMOS-inverter oscillator circuit” in Fig. 10, which had never before been used to measure strain. Since this system can measure the pulse frequency of voltage that changes according to the strain, rather than the magnitude of the voltage change, amplifiers are no longer necessary and driving power can be reduced. Because it can be powered adequately with a small battery, the system can be designed to be wireless and the equipment simplified.

Frequency of output can be described for oscillator circuit in Eq. (1),

$$f = \frac{1}{\left\{ \left(-CR \ln \frac{E - V_{TH}}{2E - V_{TH}} \right) + \left(-CR \ln \frac{V_{TH}}{E + V_{TH}} \right) \right\}} \quad (1)$$

where R is resistance of oscillator circuit, C is capacitance of condenser, V_{TH} is threshold voltage of CMOS inverter and E is applied voltage to circuit. If a strain gauge is employed to circuit as resistance, electrical resistance change is expressed by strain and gauge factor K in Eq. (2).

$$\Delta R / R = K \varepsilon \quad (2)$$

The terms higher than second order can be omitted and the following equation is obtained on referring to Eq. (1) and Eq. (2).

$$\varepsilon = -\Delta f / (f \cdot K) \quad (3)$$

Therefore, strain can be obtained by measurements of frequency change.

Static tensile tests were conducted by using new sensor system (cf. Fig. 11). Test specimen was sheet-type made of the A2024-T351 according to the ASTM E8M-04. Frequency outputs were measured during tensile loads increased statistically while strain was measured by a conventional strain sensor. Figure 12 shows the measurement results of the system being developed. The results show that strain cannot be precisely measured by using new system. The cause of error is considered as existence of internal resistance of circuit. The Equation (1) shows that product of output frequency and resistance should be constant while measurement results did not meet the relationship. However, strain values close to

those of the conventional system have been obtained due to consider the internal resistance and apply appropriate compensation factor. The corrected results are also shown in Fig. 12.

This research could find that new strain sensor with oscillator circuit was able to measure strain. In the other hands, semiconductors such as CMOS inverters are affected by thermal circumstance. In near future, thermal effects to sensor system should be considered.

3. FATIGUE AND FAILURE IN METAL/COMPOSITE HYBRID MATERIALS

3.1 Bearing Behavior of Bolted Joints in Thin Titanium Films / CFRP Hybrid Laminate

Hayato Nakatani and Shinji Ogihara
Tokyo University of Science

Mechanical fastenings using bolt-nut or rivets is one of the methods used for joining composite components for aircraft structure. However composite laminates are sensitive to stress concentration around hole or notch, and exhibit damage onset in low stress. Applications of Fiber-Metal Laminates (FMLs) for bolted joints have been researched [1]. In this article, FMLs that consist of carbon fiber composites and thin titanium films were applied to bolted joints to improve damage behavior of composite laminates. Experimental tests were conducted to examine bolted joints strength and damage behavior in the hybrid laminates with various stacking sequences.

Hybrid thin titanium-CFRP fiber metal laminates were assembled by laminating carbon fiber/epoxy prepregs (T700SC/2592, Toray) and pure titanium films (50 μ m, Sumitomo Metals Naoetsu Works), and they were cured in an autoclave. Before the lamination, titanium films were soaked in hydrogen peroxide solution of 30% as surface treatment to improve their adhesion to epoxy resin. Four types of the hybrid laminates were made by inserting several titanium films into quasi-isotropic CFRP laminates as shown in Table 1. The laminates were fastened by stainless bolts and nuts with diameter of 6mm with two cramping

CFRP plates under clamping torque of 20 Nm. Tensile loading for the bolted joint was applied to the specimen until failure under crosshead speed of 1.0mm/min.

Figure 13 shows load-displacement curves of the quasi-isotropic CFRP laminates and the hybrid laminates. There were load drop points in load-displacement curves, and they are considered to represent damage onset in the laminates. The first load drop points of the FML specimens were higher than that of quasi-isotropic CFRP laminate. In particular, the FML type C showed higher load level compared to the other FML specimens. Figure 14 shows damage in the FML specimen type A. Matrix shear cracks that follow after the fiber kinking are found to be suppressed by the thin titanium films. Based on this fact the titanium films inserted to form sandwich with 0° layers in other type of hybrid laminates to suppress the propagation of the matrix shear cracks induced by fiber kinking.

Damage in quasi-isotropic CFRP laminates and four types of FML specimens under tensile loading of 10000N are shown in Fig. 15. In the FML type B, damages induced by the fiber kinking of inner 0° layers were not suppressed, on the contrary overall damage for the FML type C kept lower level compared to the FML type B. FML type D is expected to suppress damage propagation induced by fiber kinking, however the buckling in the titanium film possibly causes damage onset in CFRP layers.

Reference

[1] B. Kolesnikov, L. Herveck and A. Fink, "CFRP/titanium hybrid material for improving composite bolted joints," *Composite Structures*, **83**, 2008, pp. 368-380.

3.2 Effects of Transition Region Structure on Mechanical Behavior of Thin Titanium Films / CFRP Hybrid Laminate

Hayato Nakatani and Shinji Ogihara

Tokyo University of Science

In case that Fibre-Metal Laminates (FMLs) are applied to joints in composite structures in order to improve their bearing behaviour, the hybrid laminates will be used locally near the bolted joints to avoid an increase in weight of the structure. In this situation it is necessary to provide "transition region" proposed by Camanho *et al.* [1], where metal volume fraction gradually decreased with the distance from the

bolt-hole. In this article, the strength and damage behaviour of the FMLs that consist of thin titanium films and CFRP plies with the transition region structure under tensile or 4-point bending loading are investigated.

The hybrid laminates were assembled by laminating carbon fiber/epoxy prepregs (T700SC/2592, Toray) and pure titanium films (50 μ m, Sumitomo Metals Naoetsu Works), and cured in an autoclave. Table 2 shows the stacking sequence of the FML specimen which is a combination of a quasi-isotropic carbon fiber composite laminates [45/0/-45/90]_{2s} and five titanium films. Four patterns of the transition region structure were evaluated here as shown Fig. 16. Here, specimens are denoted by using their stacking sequence type and the transition region pattern, for example, FML-A-1 for the stacking type A and the transition pattern 1. The hybrid laminates without the transition region, denoted by transition pattern 0, were also applied to the tests.

As shown in Fig. 17, only FML-A series were influenced by transition region pattern and FML-A-2 showed the highest tensile strength among them. Although no significant effects on the tensile strength came from the transition region pattern in FML-B and FML-C series, these specimens showed a higher strength than those of FML-A series. Delamination at three Ti/90° interfaces were observed in FML-A series, though only the central Ti/90° interface delaminated in FML-B and FML-C series. Figure 18 shows the initial damage as matrix cracking in 90° plies and interfacial delamination initiated at the edge of the titanium films inserted in the center (between 90° plies). In FML-A series these damages were also observed at all titanium edges. These damage behaviours are considered to lead to the difference in the strength of these laminates. For the 4-point bending, FML-B series showed the lowest strength because the buckling occurred at the edge of titanium films inserted near the outermost layer as shown in Fig. 19 though only CFRP plies crushed in other series. Based on these experimental facts it is concluded that the transition region structure where titanium films with staggered layout of their edges are inserted in inward side of the plate provides the best performance among tested here.

Reference

- [1] P.P. Camanho, A. Fink, A. Obst and S. Pimenta, "Hybrid Titanium-CFRP Laminates for High-performance Bolted Joints," *Composites: Part A*, **40**(12), 2009, pp.1826-1837.

4. FATIGUE AND FAILURE IN COMPOSITE MATERIALS AND COMPONENTS

4.1 Suppression of Delamination Crack for the Foam Core Sandwich Panel Joint

K. Yoshida¹, Y. Hirose¹ and A. Kuraishi²

¹ Kanazawa Institute of Technology, Ishikawa, Japan

² Kawasaki Heavy Industries, Gifu, Japan

In order to reduce the structural weight and part count, a lot of fundamental research on the application of co-cured CFRP face sheets / foamed plastic core sandwich panel to aircraft structure has been conducted. Kawasaki Heavy Industries also conducted research activities to apply foam core sandwich panel to aircraft nose structures, which was sponsored by the Japanese government. The panel joints, which are inevitable due to the restriction of the production facilities, were identified as the critical structural elements that govern the strength and fatigue life of the structure. For the configuration of the joint, a tapered end-closure type joint as shown in Fig. 20 was selected due to the easy visual inspection and convenience of fabrication and studied by Hirose et al. [1]. In this study, it was reported that the delamination crack initiating from the tapered core end and propagating through the interface between the two face sheets was observed as the initial failure mode (Fig. 20). The effect of the panel taper angle on the delamination crack initiation was experimentally evaluated and the appropriate taper angle to suppress the initial failure was investigated.

To evaluate the effect of the taper angle on the initial failure, tensile tests were conducted using the test pieces with the taper angles of 10, 20 and 30 degrees. Dimensions of the test piece are shown in Fig. 21. Face sheets consist of 16-ply graphite/epoxy twill weave fabric composite (Toho Tenax UT500/#135) laminates with nominal thickness of 6.24 mm. The ply orientations of the laminate are $[(+45,-45)/(0,90)]_4$ _{sym}. The core material is polyether imide (PEI), and the thickness is 34 mm. Resin films with thickness of 0.254 mm are inserted between the face laminate and the foam core. These resin films are extended by 5 mm to the solid laminate portion from the tapered core end. The thickness of the aluminum splice plate is 10 mm. The splice plate is installed by titanium bolts with the diameter of 7.92 mm and the spacing of 32 mm. Figure 22 shows the photos of the

test pieces. During the test, strain variations near the tapered core end are monitored and the crack propagation at the core end is visually inspected using a microscope.

Figure 23 shows the photos of the test piece with the taper angle of 20 degrees during the test. When the tensile load increased to 21.6 kN, the crack which originally propagated through the interface between the two resin films propagated into the solid laminate portion as shown in (Fig. 4(a)). In the experiments, the load when the crack propagated into the solid laminate portion was defined as the initial failure load. As the tensile load increased beyond the initial failure load, the crack propagated through the interface between the two face sheets. Fig. 23(b) shows the delamination crack which occurred at the tensile load of 32.0 kN. Measured initial failure loads are summarized in Table 3. The initial failure load increases as the taper angle decreases. Thus, the smaller taper angle is preferred to suppress the initial failure.

Therefore, to design the tapered end-closure type joint with predominantly tensile load, the taper angle should be sufficiently small so that the crack initiation and propagation at the tapered core end do not occur before other modes of failure.

Reference

[1] Y. Hirose, M. Nishitani, S. Ochi, K. Fukumoto, T. Kawasaki and M. Hojo "Proposal of suppression of delamination for the foam core sandwich panel joint with filler". *Adv. Compos. Mater.*, Vol. 15, No. 3, pp. 319-339, 2006.

4.2 Electric Characteristic Analysis of Composite Structure by Lightning Strike

Takayuki Nishi, Hiroyuki Tsubata, Hiroyasu Fujita
Fuji Heavy Industries LTD. Aerospace Company

The objective of the study is to predict the behavior for the lightning of CFRP structures that is employed to recent aircraft. With the technique it can be possible to design appropriately for the point where the problems such as electric discharges occur at a design stage, and adapted itself to the United States federal regulation of the aircraft integral fuel tank safety. The electric conductivity properties are acquired by CFRP panel and the fastener coupon for the parameter of the analysis

in this study. The analysis is developed based on FDTD method and conducted the analysis model of the box shape using basic properties that is acquired in coupon test. Then the component lightning test is conducted and test data are compared with the analysis. As a result, magnetic field strength well agreed in the range of errors less than 10% (Fig. 24).

4.3 Optical Measurement of Spark Phenomena on CFRP Specimens with Fasteners by Lightning Strike

Shinya Ohtsuka¹, Yuki Yamaguchi¹, Masaaki Furukawa¹, Takayuki Nishi², Hiroyuki Tsubata², and Hiroyasu Fujita²

¹ Kyushu Institute of Technology

² Fuji Heavy Industries LTD. Aerospace Company

This research is optical measurement of spark or discharge phenomena on CFRP (Carbon Fiber Reinforced Plastics) specimens with fasteners by lightning strike test. The CFRP specimens are reproduced on a part of main wings of the next generation airplanes made of CFRP. We constructed optical measurement system which mainly consists of a photo-multiplier tube (PMT) placed in a shield box, an optical fiber, a digital camera and antennas to estimate not only the spark generation around the faster but also the spark energy as the non-contact method. Then we applied this system to the lightning strike test and investigated the spark generation and the spark energy by changing the values of lightning current peak and the resultant wave shape. As a result, we could detect and estimate the spark generation and the spark energy by the proposed optical measurement system. (Fig. 25)

This research was a part of the project, “Advanced System Technology for Aircraft” under the contract with Ministry of Economy, Trade and Industry.

4.4 Evaluation of Notched Strength and Damage Behaviour in Non-crimp Fabric Based Composites

Hayato Nakatani¹, Shinji Ogihara¹, Nobuo Takeda², Yuichiro Aoki³, Shin-ichi Takeda³ and Yosuke Nagao⁴

¹ Tokyo University of Science

² The University of Tokyo

³ Japan Aerospace Exploration Agency (JAXA)

⁴ Kanagawa Institute of Technology

In order to establish a damage tolerance design for the latest composite aircraft fuselage structure testing and numerical analysis for various scales from basic tests to full scale model are in progress mainly in Japan Aerospace Exploration Agency. Characterization of tensile properties of carbon fiber composites containing stress concentration such as notch is necessary for the damage tolerance design assuming scattering of engine debris that penetrates the structure. Composites manufactured by Vacuum assisted Resin Transfer Molding (VaRTM) have been applied to aircraft structure recently, and non-crimp fabrics (NCFs) are often used in the VaRTM process. This fabric consists of individual plies stitched together by a polyester yarn, and this makes its structure different from that of common fabric and results in decrease fiber waviness and smooth flow of resin in molding process. In this article, tensile tests are conducted using the NCF based composites containing a notch to evaluate their mechanical properties and damage behavior, and they are compared to those of prepreg laminates.

Tensile strength and damage behavior in the NCF (SAERTEX, carbon fibre: STS40, Toho Tenax) based composites $[(45/-45)/(0/90)]_{2S}$ with a centrally located notch were compared to that of the conventional prepreg laminates $[(45/-45/0/90)]_{2S}$, STS40/#11B, Toho Tenax). The notched strength of the NCF based composites normalized by its unnotched strength was comparable with that of the prepreg laminates though it showed some variation between individual specimens. This was found to be due to the inhomogeneous ply thickness, stacking state, and stitch yarn used in the NCFs. It was observed that the stitch yarns induced the resin rich spots and porosities around them and they also contributed to the unstable damage mode. The well-known point stress criterion (PSC) [1] that has been used to predict the notched strength of conventional prepreg laminates was applied to the NCF based composites. PSC is confirmed to be valid for the NCF based composites to predict their notched strength using same characteristic length as of the prepreg laminates without any modification as shown in Fig. 26.

One can notice that positional relationship between the notch edge and stitch site (Fig. 27) will affect the stress state near the notch edge and also notched strength of the laminates. Stress distributions near the notch edge with the resin

rich spots were calculated by finite element analysis. Three cases were considered here as shown in Fig. 28. Those represent that there are no resin rich spot near the notch edge (case 1) and the spot is just on (case 2) and 0.3 mm ahead of the notch edge (case 3). From the calculated stress in 0° ply (Fig. 29) it was obvious that there was a difference in the maximum stress for case 1 at the notch edge and for case 2 at fiber-resin interface, and stress concentration at the notch edge for case 3 was higher than for case 1. For case 3 stress kept high level at between the notch edge and the fiber-resin interface compared to other cases, one can expect that damages would tend to initiate in this portion. From these facts it was confirmed that the stress distributions were affected by the spots and resulted in variation in the notched strength of the NCF based composites.

Reference

[1] J.M. Whitney and R.J. Nuismer, "Stress Fracture Criteria for Laminated Composites Containing Stress Concentrations," *Journal of Composite Materials*, 8, pp. 253-265, 1974.

4.5 Effect of Fiber Volume Fraction on First Transverse Crack Formation in Cross-Ply CFRP Laminates under Fatigue Loading

Atsushi Hosoi¹, Ko Shigemori², Yuzo Fujita³ and Hiroyuki Kawada²

¹ Nagoya University, Japan

² Waseda University, Japan

³ Toray Industries, Inc., Japan

Carbon fiber reinforced plastic (CFRP) has been used as a primary structural members of a commercial airplane, and B787 realizes 20 % reduction in fuel consumption in comparison with a conventional airplane. At present, the ultimate design strain level in aircrafts are kept low, in the region of 5000 $\mu\epsilon$, where composite materials can withstand large numbers of fatigue cycles without failing, thus at this strain level damage growth is not seen as a major problem. However, to use composite structures to their full potential, design strain levels will have to rise and a partial growth criteria needs to be adopted. Especially, a transverse crack is generally first damage in CFRP laminates and it induces more serious damage, such as delamination or fiber breakage. It is essential to understand the mechanism of the transverse crack initiation for improving long-term durability of CFRP

laminates. Recently, the authors proposed new approach to predict first transverse crack formation quantitatively under fatigue loading¹⁾ and evaluated the effect of ply thickness on the first transverse crack formation²⁾. However, the effect of the fiber volume fraction on the first transverse crack formation under fatigue loading has not been cleared. Thus, the effect of the fiber volume fraction on the first transverse crack formation was evaluated quantitatively by using the cross-ply CFRP laminates with two different fiber volume fractions of $V_f=61\%$ and 68% .

The first transverse crack formation is predicted by evaluating asymptotically the multiplication behavior of transverse cracks, which can be evaluated by using the relationship between the transverse crack density growth rate and the energy release rate range associated with transverse crack formation under fatigue loading. The proposed model show good agreement with experimental results (Fig. 30). By using the model, the effect of the fiber volume fraction on the first transverse crack formation was evaluated (Fig. 31). From the figure, it was cleared that the fatigue life to the first transverse crack formation in the laminates with high fiber volume fraction is longer than that in the laminates with low fiber volume fraction in high-cycle region. Under fatigue loading, the transverse crack was formed meandering along the interface between fiber and matrix (Fig. 32). Thus, the crack area of the transverse cracks in the laminates with high volume fraction becomes larger than that with low fiber volume fraction, and that means that the larger energy is needed for the transverse crack growth in the laminates with high fiber volume fraction. The effect will be considerable in high-cycle region. Therefore, the fatigue life to the first transverse crack formation in the laminates with higher fiber volume fraction becomes longer in high-cycle region.

References

- 1) Hosoi, A. et al. (2012), *Trans. Jpn. Soc. Mech. Eng. A*, vol. 78, n. 791, p. 1000. (in Japanese).
- 2) Hosoi, A. et al. (2012), *Proceedings of ACCM8*, Paper n. O-FRA-027.

4.6 Durability Evaluation of Carbon/BMI Composites After Thermal Aging (DECATA)

H. Katoh¹, D. Lévêque², K. Hasegawa³, J. Cinquin⁴

¹ Japan Aerospace Exploration Agency (JAXA), Tokyo, Japan

² ONERA, Châtillon, France

³ Mitsubishi Heavy Industries, LTD., Nagoya, Japan

⁴ EADS-IW, France

This article synthesizes all the results obtained during the Japanese-French cooperation on the supersonic aircraft transport – under the SJAC-GIFAS Frame Agreement – and concerns the durability evaluation of Carbon/Bismaleimide (BMI) composites after thermal aging. The long-term behavior is a major topic to use composite materials such as aircraft structures over twenty or thirty years in service-life. New organic composite materials can satisfy these requirements but they must undergo physical and mechanical tests to be qualified.

Durability aspect of organic composite materials is a very complex problem since it comprises multi-disciplinary effects coming from various and numerous factors such as temperature, pressure, oxygen, moisture, radiation, polluted volatiles as well as mechanical stresses in service-life. In standard applications, structural composites evolve in air for flight time and the two main aging factors are heat and oxidizing atmosphere. Actually, we are dealing with a combination between temperature and oxygen effects. This combination gives rise a damage which is a consequence of chemical and physical aging undergone by the organic matrix. Consequently, to meet the problem on durability, it is necessary to appeal both physics of polymers and mechanics of composite materials. The aim of this research program is to value the physical and mechanical properties taking into account damages occurring under various thermal conditions in order to predict the long-term behavior.

Two kinds of composite laminates from the same BMI family have been selected: the first one is MR50K/2020 system (Mitsubishi Rayon Ltd); the second one is IM7/M65 system (Hexcel Composites).

Isothermal conditions in air have been performed at 150, 180 and 200°C for several thousands hours (from 1,500 up to 10,000 hours) at each temperature and for both composite materials.

The mechanical characterization is performed by fracture toughness tests at a macro-scale on DCB specimens and off-axis tensile tests on $[+45/-45]_{2S}$ laminates. Moreover, the compressive strength of non-hole (NHC) and open-hole (OHC) $[+45/0/-45/90]_{4S}$ QI specimens is determined for each thermal aging condition defined at the three temperatures. The physical tests consist on following the glass

transition temperature (T_g) and measuring the weight loss evolution on UD specimens.

Figure 33 shows the weight loss during aging. The weight decreases by isothermal aging at any temperature. The amounts of weight loss are almost same between both laminates. The weight losses are clearly related to the aging temperature. It seems caused by accelerated diffusion of oxygen through the surface, where the matrix is degraded by the thermo-oxidation reaction.

Figure 34 shows the T_g evolution after aging. The T_g was monotonically increased with aging time, the degree of evolution is significant in higher aging temperature. The increase seems to be brought about by what is called post cure effect, which is a further enhancement of cross-linking density due to the reaction of remaining functional groups.

Figure 35 shows the G_{Ic} evolution after thermal aging. The G_{Ic} dramatically decreased when aged at 150°C up to 1,500 hours and are not related to the aging temperature. Over 6,000 hours the G_{Ic} values do not meaningfully reflect the interlaminar toughness degradation because propagation of the delamination between other layers was prominently generated during testing. Significantly the delamination propagated near surface. Therefore, the delamination seems to be propagated by accelerated diffusion of oxygen through surface. However, it is not fully understood why there is no big difference among aging temperatures.

In the particular case of aged DCB specimens, some longitudinal cracks (in the 0°-plies) may have been created during aging under constant residual stresses condition. The toughness of the composites have significantly degraded properties in the first aging time probably due to post cure effects (the cross linking density increase but the brittleness of the matrix too) as shown by the T_g evolutions for the same times. The re-rising of G_{Ic} values for longer aging times is more related to multiple damages formed during testing that contribute to the energy absorption by a significant fiber bridging. At last, the off-axis tensile modulus is slightly affected by the thermal degradation but with a constant decrease versus time.

In this study, some relationships between damage and respective residual mechanical properties have been established for two carbon/BMI systems. Some issues remain, in particular the shared role between thermal aging effects, residual thermal stresses and mechanical loading.

4.7 Application of Bayesian Analysis to Determining Fatigue Load on Composite Structures

Seiichi Ito, Sunao Sugimoto and Takao Okada

Japan Aerospace Exploration Agency (JAXA), Tokyo, Japan

The load enhancement factor (LEF) approach is proposed as a fatigue acceleration test to demonstrate the fatigue strength of composite material structures. Some experiments on the full-scale composite structure are executed based on this method. In the LEF method, the probability distribution of residual strength and fatigue life is assumed to be two parameter Weibull distribution, respectively. The result of LEF by statistical approach is defined as a function of shape parameters from the Weibull distributions. Then, the uncertainty of residual strength and fatigue life greatly affects the load enhancement factor assessment. In this report, Bayesian analysis is applied to estimation for the uncertain factors to evaluate LEF. In addition, a probabilistic model which can determine the reasonable fatigue load is explained. And this research deals with the Bayesian expected LEF and its comparison with already reported results in Composite Materials Handbook (CMH-17).

Conventional LEF approach (CMH-17)

Evaluation model for the LEF method is illustrated in Fig 36. The object of LEF approach is to increase the applied loads in the fatigue spectrum so that the same level of reliability can be achieved with a short test duration. As mentioned previously, the probability distribution of fatigue life L and residual strength r is given by Weibull distribution, $W(L|\alpha_L, \beta_L)$ and $W(r|\alpha_r, \beta_r)$, respectively. A final mathematical relationship of LEF is shown by equation (A1) of Fig. 37. For the sake of simplicity, the modal values of α_L and α_r calculated from the database are applied in equation (A1).

Reassessment of LEF based on Bayesian analysis

The shape parameter α is modeled as a probability distribution by using the procedure of the Bayesian analysis to evaluate the scatter of the shape parameter. The Shape parameter α is estimated from the structural test database, using the procedure of the Bayesian analysis. Log-normal distribution of $LN(\alpha_L|\mu_L, \sigma_L^2)$ and $LN(\alpha_r|\mu_r, \sigma_r^2)$ are assumed for the probability distribution of shape parameters, α_L and α_r , respectively. The mean μ and variance σ^2 for the distribution are assumed to be unknown parameters. By using the database and Bayesian conjugate analysis

the posterior distributions $h(\mu_L, \sigma_L^2)$ and $h(\mu_r, \sigma_r^2)$ of the uncertain parameters are obtained. The marginal distribution function of α is calculated by summing the joint probabilities over all of the possible values of μ and σ^2 . The notation of the marginal distribution for α_L and α_r are $f(\alpha_L)$ and $f(\alpha_r)$, respectively. By introducing the above results, the average LEF is defined in equation(A3) as shown in Fig. 37. The LEF in the equation shows so-called Bayesian expected value of LEF.

Comparison of Conventional LEF with Bayesian LEF(LEF)

Because the mode value of α is smaller than that of the mean value, the mode is used in the calculation of LEF in CMH. However, as LEF is a function of α_L and α_r , the expected value of LEF is led in this analysis. A result of the expected value of LEF is shown in Table 4. The LEF is larger than LEF that uses the mode value in CMH. The range of integration of LEF was calculated here by three cases in consideration of the realistic value region of the shape parameters, α_L and α_r . The LEF indicates the value of the safety side compared with the conventional LEF though LEF depends within the realistic range of integration to shape parameters.

5. STRUCTURAL HEALTH MONITORING

5.1 Hierarchical Fiber-optic System for Detecting Impact Damage in Large-scale Composite Structure

Shu Minakuchi and Nobuo Takeda

The University of Tokyo

Optical fiber sensors have attracted a considerable amount of attention in the structural health monitoring (SHM) field, since they are small, lightweight, immune to electromagnetic interference, environmentally stable, and have very little signal loss over extremely long distances. Previous studies have successfully demonstrated that fiber-optic-based systems are highly sensitive to wide-ranging damage modes in advanced composite materials represented by carbon fiber reinforced plastic (CFRP) [1]. However, when the conventional fiber-optic-based systems (Fig. 38 (a)) are applied to large-scale structures for monitoring randomly induced damage such as impact damage [2], they are unsatisfactory in the following three properties: robustness, repairability, and monitorable area.

Specifically, a failure at only one point on a sensing optical fiber leads to a breakdown of the entire sensing network. Moreover, once the optical fiber is disconnected, the damaged part needs to be repaired. However, it is quite difficult to access and reconnect the damaged fiber. Furthermore, the fiber-optic sensing obtains basically a one-dimensional strain (temperature) distribution along the thin fiber. Hence, damage far from the sensing fiber cannot be detected, since it induces no significant strain (temperature) change in the fiber.

To overcome these drawbacks, this study proposed a hierarchical fiber-optic-based sensing system analogous to the nervous system in vertebrates [3]. In the hierarchical system (Fig. 38 (b)), several kinds of specialized devices are hierarchically combined to form a sensing network. Specifically, numerous three-dimensionally structured sensor devices are distributed throughout the whole structural area and connected with an optical fiber network (which is not embedded into the structure) through transducing mechanisms. The distributed “sensory nerve cell” devices detect damage, and the fiber-optic “spinal cord” network gathers the damage signals and transmits the information to a measuring instrument. Since the optical fiber is attached to the back surface of the structure, the fiber rarely breaks when the structure is damaged. If by any chance the optical fiber is broken, the disconnected parts can be readily reconnected using a fusion splicer, since the optical fiber is relatively easily accessible. Finally, in the hierarchical system, several sensor devices connected to different optical fibers are placed in the same area; in Fig. 38 (b), two independent comb-like sensor devices share the same monitoring area. Hence a failure at just one point in the devices or the fiber optic network does not affect the monitoring performance, and therefore the hierarchical system has high redundancy and robustness.

In order to validate the hierarchical concept, a hierarchal impact damage detection system was developed (Fig. 39). The distributed sensor devices are based on comparative vacuum monitoring (CVM) [4]. The CVM system, which was developed by Structural Monitoring Systems Ltd. in Australia, uses an elastomeric surface sensor with fine channels that detects surface cracks by monitoring internal pressure variations in the channels. Basically, CVM technology has been applied to monitor localized areas such as joining parts and bonding lines. In this study, however, tightly arranged devices are bonded onto the back surface of a composite structure. The sensor device consists of thin fibers covered with air-tight tapes (A in Fig. 39). The size of the device is identical to the spatial resolution of the

damage detection system, and the interval between the air-tight tapes is determined by the unacceptable impact damage size, depending on the structural site. The space between the fiber and the tape is maintained as a vacuum and is utilized as a sensing channel. The sensor devices are connected to the optical fibers via damage signal transducing mechanisms (B in Fig. 39). Specifically, a rigid plastic tube is connected to the sensing channels of the distributed sensor device, and the optical fiber is fixed in the tube through a movable part. The mechanism converts the internal pressure variation of the distributed sensor device into an axial strain change in the optical fiber. When impact damage is induced, a bending crack appears along the reinforcing fiber direction on the back surface, just below the impact point [2]. The surface crack forms a leakage path between the atmosphere and the distributed sensor devices, increasing the internal pressure in the sensing channel and thus in the connected plastic tube. The pressure increase then pushes the movable part and induces shear deformation of the soft polymer inserted between the movable part and the plastic tube and consequently applies axial strain to the optical fiber. The strain distribution along the optical fiber is monitored by using a distributed strain measurement system (e.g., a Brillouin-based system [5]). Therefore, one can easily identify the transducing mechanism and sensor device where the pressure change occurred, and thus locate the damaged area.

The proposed impact damage detection system was applied to a CFRP skin-stringer fuselage demonstrator (Fig. 40 (a)). Barely visible impact damage (BVID) was successfully detected from the strain increase in the optical fiber at the damaged area (Fig. 40 (b)), clearly confirming that the hierarchical system has better repairability, higher robustness, and a wider monitorable area compared to existing fiber-optic-based systems [3].

References

- [1] Takeda, N., Okabe, Y., and Mizutani, T. (2007) "Damage detection in composites using optical fibre sensors," Proceedings of the Institution of Mechanical Engineers Part G - Journal of Aerospace 221(G4) 497.
- [2] Abrate, S. (1998) *Impact on Composite Structures*, Cambridge: Cambridge University Press.
- [3] Minakuchi, S., Tsukamoto, H., Banshoya, H., and Takeda, N. (2011) "Hierarchical fiber-optic-based sensing system: Impact damage monitoring of large-scale CFRP structures," *Smart Materials and Structures* 20(8) 085029.
- [4] Structural Monitoring Systems Ltd 2013 <http://www.smsystems.com.au/>
- [5] Neubrex Co., Ltd 2013 <http://www.neubrex.com>

5.2 Development Status of Structural Health Monitoring Technologies Using Optical Fiber Sensors at MHI

Takashi Yari¹, Nozomi Saito¹, Satoshi Matsuura², Yoshihiro Kumagai², Kazuo Hotate³, Kiyoshi Enomoto⁴

¹ Mitsubishi Heavy Industries, LTD.

² Yokogawa Electric Corporation

³ The University of Tokyo

⁴ Sokeizai Center

Brillouin optical correlation domain analysis (BOCDA) is suitable method for aircraft structure health monitoring, because BOCDA is able to measure strain distributions of large area and dynamic strain on arbitrary points. The BOCDA-SHM system application concept is shown in Fig. 41. Whole structure strain distribution is monitored by BOCDA device and evaluates structural health from strain change. The goal of our activity is to put practical use for the BOCDA-SHM system. The authors conducted several experiments and verified several technologies¹⁾, for example, BOCDA measuring technology development and enhancement, assembled the prototype BOCDA measuring device for commercial airplane use, developing structural damage detection method and assessing its ability and reliability, and environmental and mechanical durability evaluation of installed into/ onto structure optical fiber sensors. In this paper, we introduce application tests for composite structure.

Firstly, de-bonding damage is one of the critical damage in composite structure. We conducted the de-bonding detect test. The overview of the test article and test condition is shown in Fig. 42. The test specimen was CFRP panel with the strap simulated stringer flange. The size of the test specimen was 1000mm in length, 400mm in width, and 8ply (about 1.52mm) in thickness. The strap (400mm x 50mm) was secondary bonded on the plate. The tension force was increased step-by-step, and distributed strain was measured at each step with 30mm spatial resolution. The measured distributed strain is shown in Fig. 43. The optical fiber section of 15.8m~16.5m was near bonded strap. The de-bonding damage was occurred at the 130kN tension load. The distributed strain changed at the 15.95m. The de-bonding damage propagation was able to identify by strain distribution. We developed the diagnosis technique using Mahalanobis Taguchi (MT) system same diagnosis method with the delamination

detection techniques. The differential from the above method was employed for diagnosis parameters. The employed parameters in the de-bonding damage detection method were Brillouin frequency shift (BFS) distributions and wavelet coefficient of its BFS distribution. The MT diagnosis result is shown in Fig. 44. This figure describes the Mahalanobis distance (MD) distribution along optical fiber sensor. The diagnosis results indicate MD increased at the de-bonding damage occurred portion.

Secondly, bolted joint portion is one of the most important portions for structure inspection. In the composite structure, the main failure mode at bolted joints is bearing failure. Bearing failure occurs from the micro-damages such as the fiber micro-buckling, matrix cracking, out-of-plane shear cracking and interlaminar delamination. These bearing damage occurrences and expanding in composites laminates were detected by the BOCDA-SHM technology. The specimens used in the bearing damage tests were multi-fastener single-lap CFRP laminates as shown in Fig. 45. The specimens were CFRP quasi-isotropic laminates ($[45/0/-45/90]_{2S}$) with embedded optical fiber sensor. The specimen width, length and thickness were 150 mm, 350 mm and 16 plies (about 3 mm), respectively. The optical fiber sensor was embedded into two interlayers, paralleled to the fastener line, A and B. Figure 46 shows the Brillouin gain spectrum (BGS) shapes along the optical fiber near center bolt. Dotted line, dashed line and solid line in this figures show the BGS measured before micro-damages occurred (1), after micro-damages occurred (2) and after micro-damages expanded (3), respectively. In this paper, only the BGS results were showed because the BFS distributions were not changed before and after micro-damages occurred. According to the BOCDA measurement result and microscopic observations, it would be said that a BOCDA optical fiber sensor embedded in interlayer-A $[90^\circ/\text{fiber}/90^\circ]$ has a high probability of detection compared with that embedded in interlayer-B $[0^\circ/\text{fiber}/-45^\circ]$ though interlayer-B is the nearest layer from 0° layer, where fiber-buckling that occurs at an early stage of bearing failures.

This work was conducted as a part of the project “Aerospace Industry Innovation Program – Advanced Materials & Process Development for Next-Generation Aircraft Structures” under the contract with The Material Process Technology Center (SOKEIZAI Center), founded by Ministry of Economy, Trade and Industry (METI) of Japan.

Reference

- 1) T. Yari, M. Ishioka, K. Nagai, M. Ibaragi, K. Hotate and Y. Koshioka, Mitsubishi Heavy Industries Technical Review, Vol. 45, No.4 (2008) pp. 5-8.

6. FULL-SCALE TESTING

6.1 XP-1/XC-2 Full Scale Strength Test

T. Okazaki

Air Systems Research Center, Technical Research and Development Institute (TRDI), Ministry of Defense, Japan

TRDI has been conducting simultaneous development of the next-generation maritime patrol aircraft (XP-1) and the next-generation cargo transport (XC-2). XP-1 is the successor of P-3C aircraft currently operated by Japan Maritime Self-Defense Force, and XC-2 is the successor of C-1 operated by Japan Air Self-Defense Force. The contractor of the development program is Kawasaki Heavy Industries, Ltd.

The FSST (Full Scale Static Test) consists of the limit load tests and the ultimate load (1.5 times the limit load) tests. It is to demonstrate static strength of airframe by simulating a variety of design loads, such as maneuver, gust, and landing loads, using lots of actuators controlled synchronously.

The FSFT (Full Scale Fatigue Test) consists of the durability test and the damage tolerant test. Durability test was conducted for twice the design service life of spectrum loading for validation of the airframe structure.

The damage tolerance test was started from the state with the initial flaws, residual strength test was conducted after twice the design service life spectrum load (Fig. 47 and Fig. 48)

FSST and FSFT (durability test and damage tolerance test) for XP-1 is expected to end early in 2013.

FSST and FSFT of XC-2 is expected to continue to demonstrate strength of the aircraft structure.

6.2 Manufacturing Demonstration of a Prepreg - VaRTM Hybrid Composite Aircraft Part and Its Evaluation

Sunao Sugimoto¹, Yutaka Iwahori¹, Sho Miyashita², Kazushi Sasaki², Yasunari Kuratani³, and Kenjiro Asano³

¹Japan Aerospace Exploration Agency

²ShinMaywa Industries, Ltd.

³KADO Corporation

The excellent mechanical properties of carbon fiber compared to other materials have established prepreg technology in the aerospace field. Several properties of composite material are ideally suited to the mission requirements of flight safety and extended flight times. The most essential of these properties are corrosion resistance and lighter weights with greater strength compared to metal. Composite material will be used for about half of the weight of the state-of-the-art passenger plane. Compared to conventional planes, the latest developed airplane is expected to fly over longer distances with improved mileage due to reduced airframe weight, and its superior corrosion resistance is expected to endow it with a stronger body and better cabin environment. However, technical difficulties remain in manufacturing complex structures such as sections with integrated stringers and frames, further which leads to high cost. The cost is tremendously high in terms of both time and money. A typical CFRP structure molding method for aircraft is the autoclave molding process by using unidirectional carbon fiber prepreg. Though prepreg is quite suitable for fabricating simple structure with high quality, this fabrication process requires expensive autoclave equipment, which entails high fabrication costs.

Japan Aerospace Exploration Agency (JAXA) has been pursuing the development of a cost efficient composite fabrication technology for innovative aerospace structures. A completed five-year VaRTM (Vacuum-Assisted Resin Transfer Molding) wing box development project (between 2004 and 2008) has demonstrated that VaRTM technology provides sufficient quality as well as structural performance to satisfy aircraft design requirements at 25% lower fabrication cost than prepreg structures. In the VaRTM process, molding and curing are carried out under atmospheric pressure by using dry fabric (i.e. dry preform) without the use of autoclave equipment. The process using dry preform is more flexible to make complicated structure compared with conventional prepreg

layup approach. However, the quality of the VaRTM fabrication tends to be affected by the method of resin infusion and the size and shape of the structure, where the technical experiences, so-called 'know-how' is dominant factor. This makes it quite challenging to fabricate larger and more complex structures by VaRTM process. Recently, JAXA is focusing on a VaRTM and Prepreg Hybrid (VPH) process to reduce manufacturing costs.

The proposed VPH process is an innovative one-shot fabrication technology that combines the advantages the prepreg and VaRTM techniques. In the VPH process, advantages of each technique are used to fabricate more complex integral airframe structures without autoclave equipment, at much lower cost than conventional methods.

A metal speedbrake of Sabreliner 80 (North American Aviation, Inc.) business jet, shown in Fig. 49, was selected and redesigned with VPH fabrication technique as a technology demonstrator. Although the original metal speedbrake is a skin-stringer structure, the composite speedbrake has CFRP skin sandwich panel with Al 7075 bar parts as shown in Fig. 50. The CFRP sandwich panel was made with an outer skin of out of autoclave prepreg, a foam core of ROHACELL, and an inner skin of VaRTM CFRP. Used materials for the speedbrake is shown in Table 5. This sandwich panel was cured at one time in an oven and assembled with metal parts. The manufactured composite speedbrake demonstrate about 30 % weight and 1/10 parts count reduction from original metal speedbrake. The composite speedbrake was applied ultimate load of the most critical load case from structural load report of Sabreliner 80 by pressure of air mats shown in Fig. 51. The composite speedbrake withstand the ultimate load and a load-strain curve of the highest strain points, points 15, 16, 17, 18 in Fig. 50, is shown in Fig. 52. The average of maximum strain at those points was about 3100 $\mu\epsilon$. The composite speedbrake demonstrator shows the potential ability of VPH process to reduce the weight and parts number significantly.

ACKNOWLEDGEMENTS

The editors appreciated the members of the ICAF national committee of Japan Society for Aeronautical and Space Sciences, for their contribution in preparation of this national review and continuing discussion in the committee.

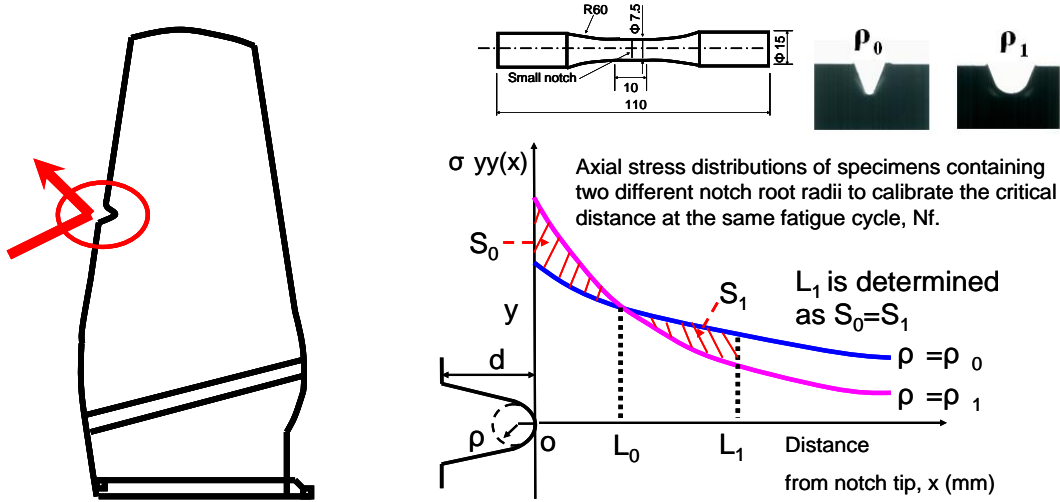
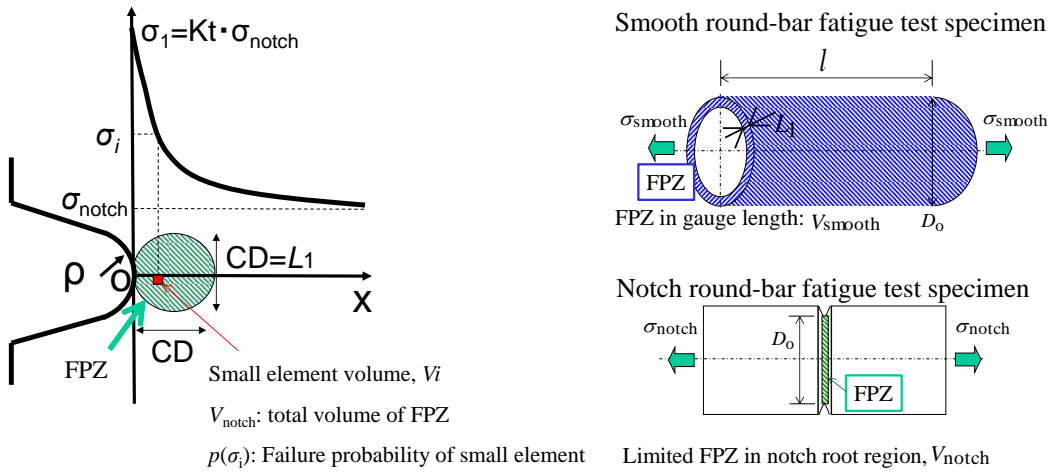


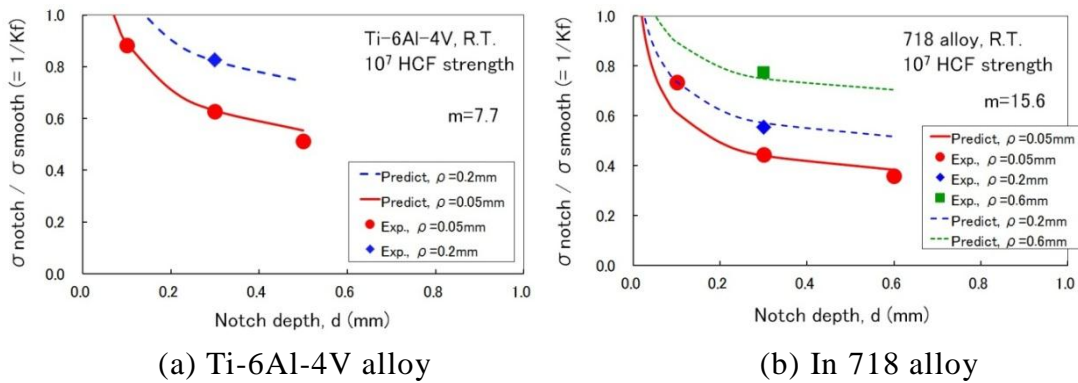
Fig. 1 Schematic of small notched fan blade and calibration of critical distance



(a) FPZ in notch specimen

(b) Difference in FPZ between smooth and notch specimens

Fig. 2 Schematics of fracture process zone



(a) Ti-6Al-4V alloy

(b) In 718 alloy

Fig. 3 Predicted fatigue notch factor derived from the weakest link theory using critical distances

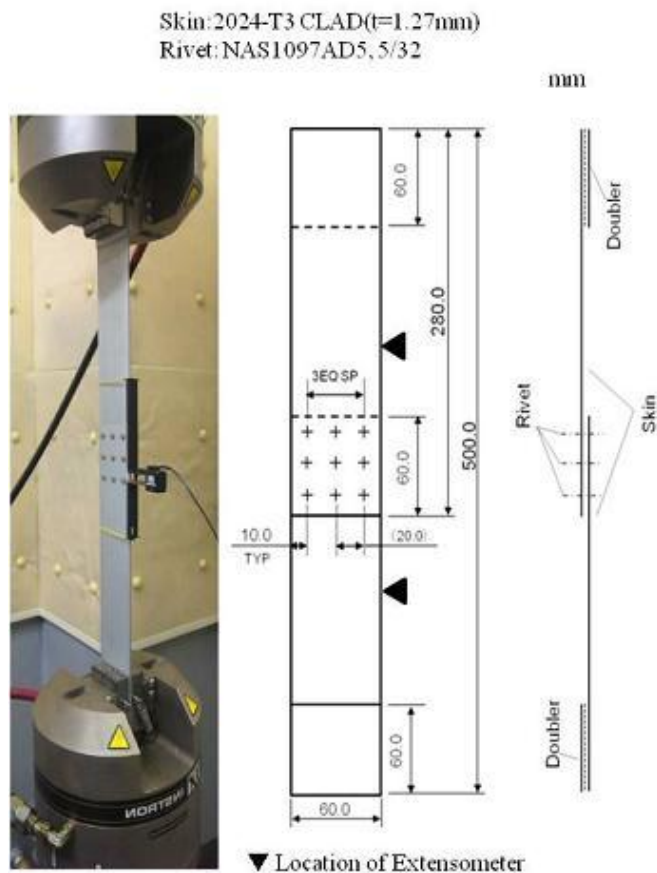


Fig. 4 Test specimen

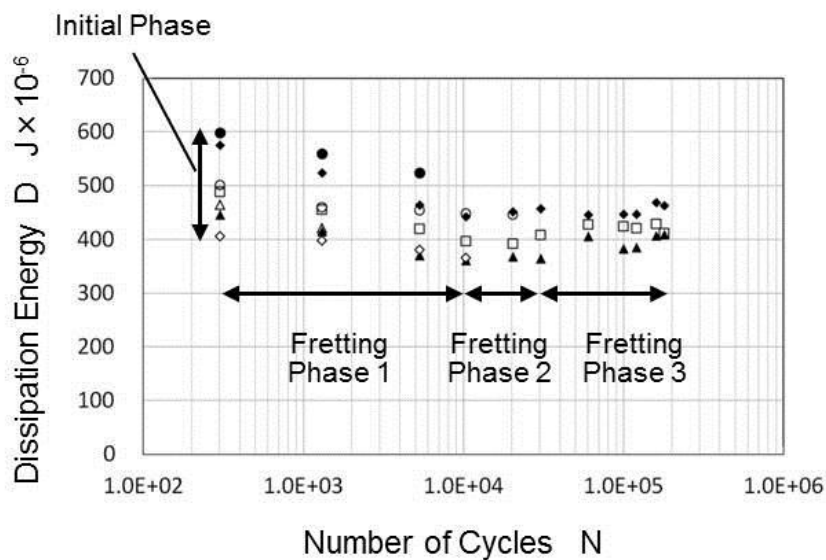


Fig. 5 Dissipation energy per cycle

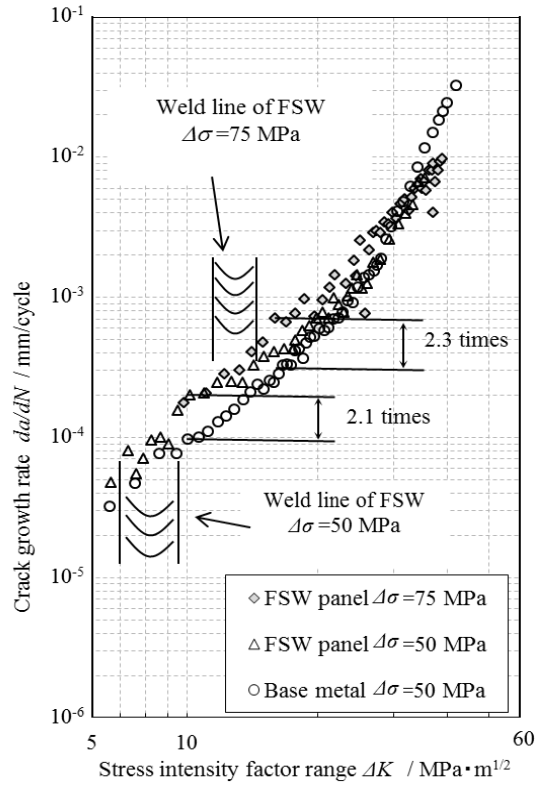


Fig.6 Fatigue crack growth rate of FSW specimen at $\Delta\sigma = 75$ and 50MPa

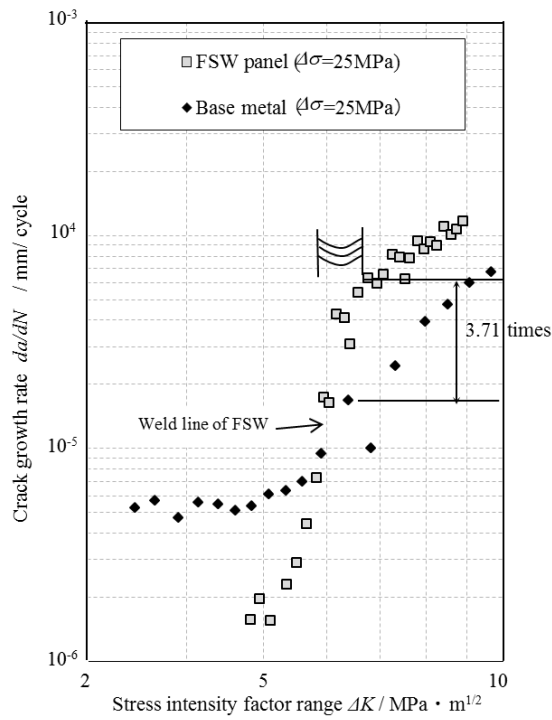


Fig. 7 Fatigue crack growth rate of FSW specimen at $\Delta\sigma = 25$ MPa

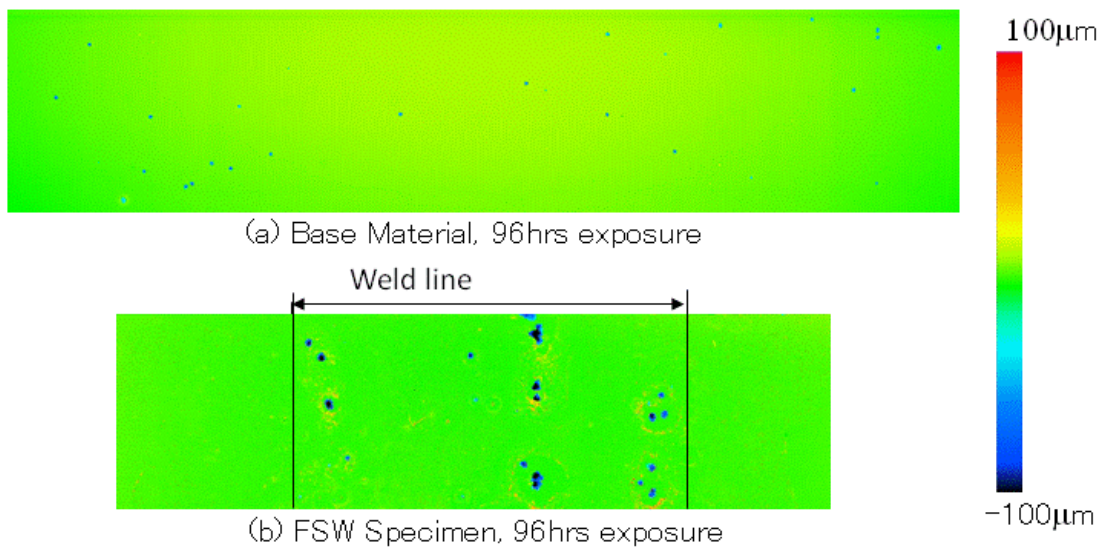


Fig. 8 Corroded surface of specimen

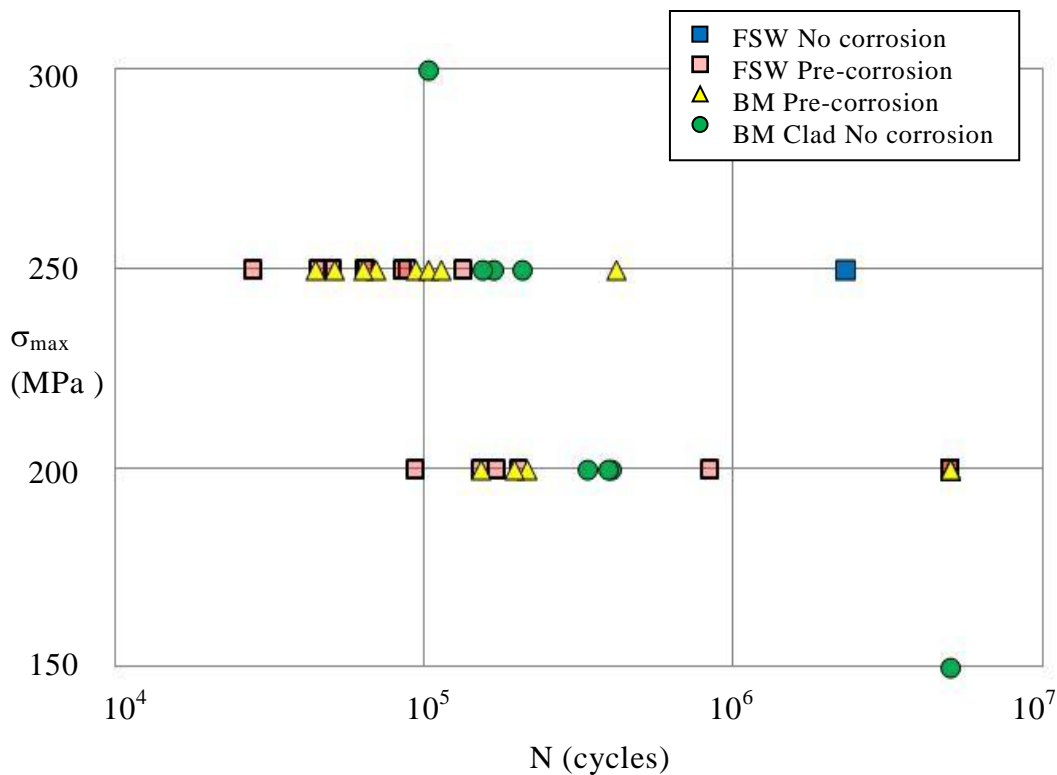


Fig. 9 Fatigue test result of pre-corroded specimen

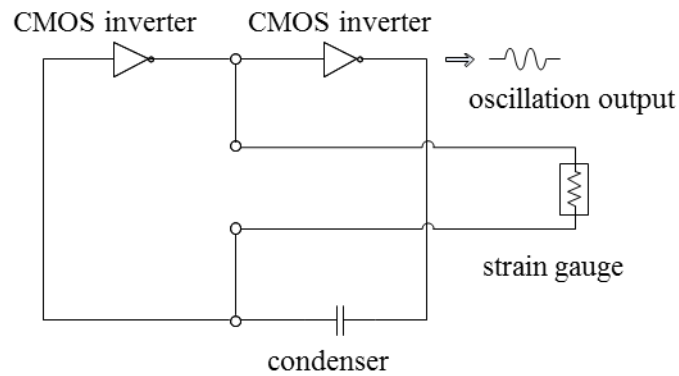


Fig.10 CMOS-inverter oscillator circuit



Fig. 11 Tensile test

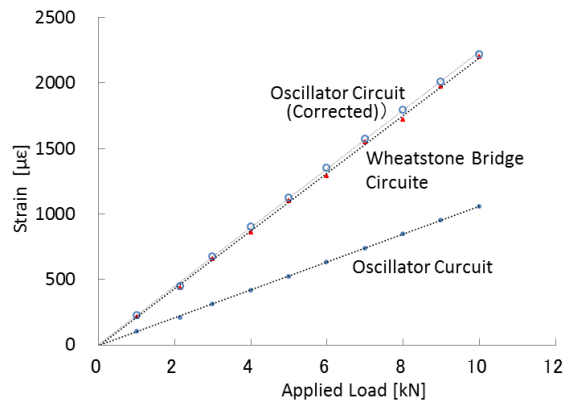


Fig. 12 Test results

Table 1 Stacking sequence of the laminates tested.

Specimen	Stacking sequence	Areal density [g/cm ²]
CFRP	[45/0/-45/90] _{2s}	0.35
FML-A	[45/0/-45/Ti/90/45/0/Ti/-45/90/Ti/90/-45/Ti/0/45/90/Ti/-45/0/45]	0.46
FML-B	[45/Ti/0/Ti/-45/90/45/0/-45/90/Ti/90/-45/0/45/90/-45/Ti/0/Ti/45]	
FML-C	[45/0/-45/90/45/Ti/0/Ti/-45/90/Ti/90/-45/Ti/0/Ti/45/90/-45/0/45]	
FML-D	[45/Ti /0/Ti /-45/90] _{2s}	0.52

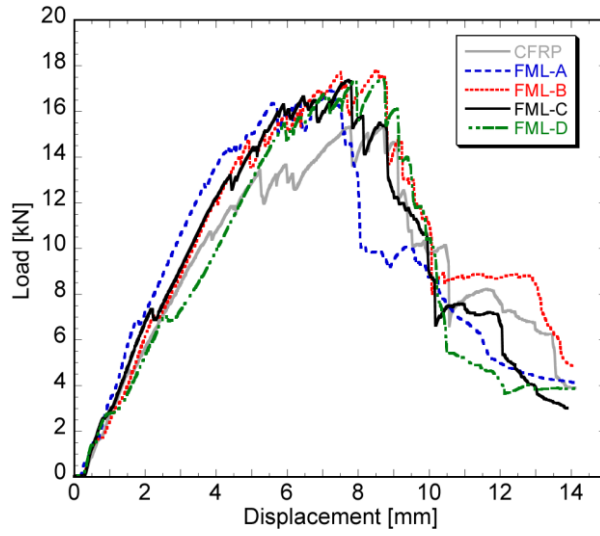


Fig. 13 Load-displacement curves of bolted joint tests

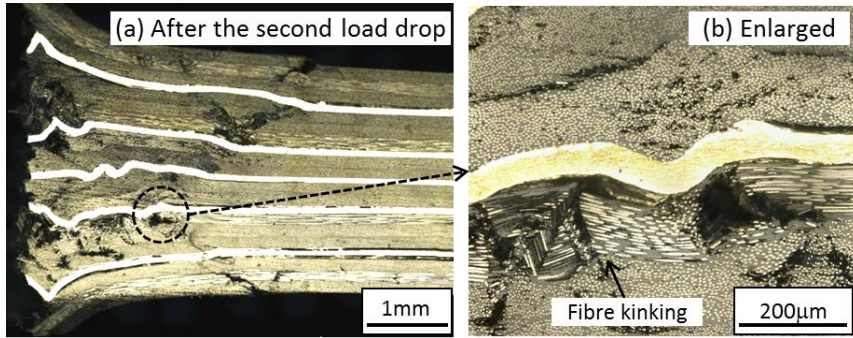


Fig. 14 The titanium film prevents the matrix cracking to propagate into adjacent layers. (FML type A)

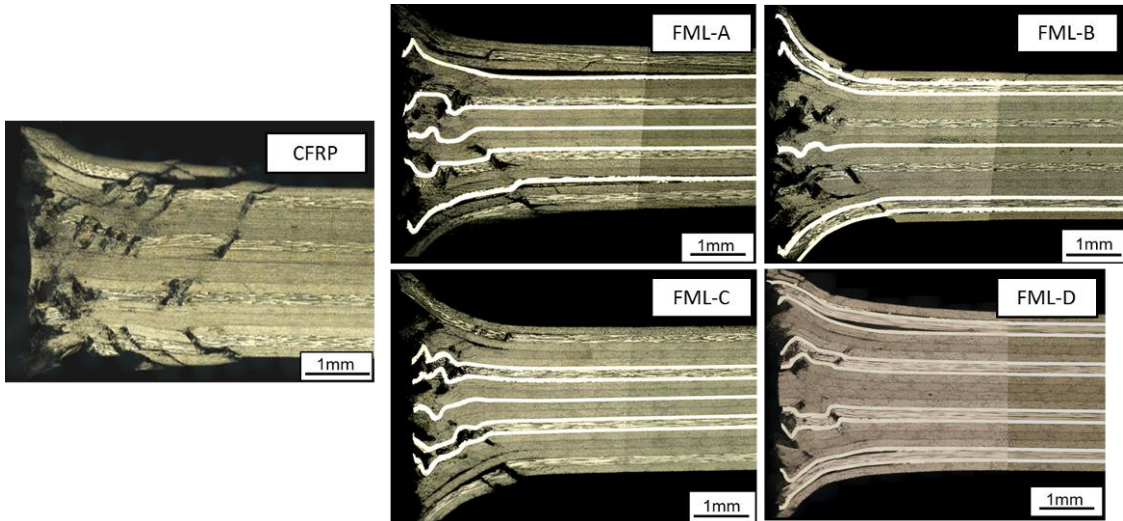


Fig.15 Bearing damage in the FML specimens under tensile load of 10000N

Table 2 Stacking sequence of the laminates used

CFRP	$[45/0/-45/90]_{2S}$
FML-A	$[45/0/-45/Ti/90/45/0/Ti/-45/90/Ti/90/-45/Ti/0/45/90/Ti/-45/0/45]$
FML-B	$[45/Ti/0/Ti/-45/90/45/0/-45/90/Ti/90/-45/0/45/90/-45/Ti/0/Ti/45]$
FML-C	$[45/0/-45/90/45/Ti/0/Ti/-45/90/Ti/90/-45/Ti/0/Ti/45/90/-45/0/45]$

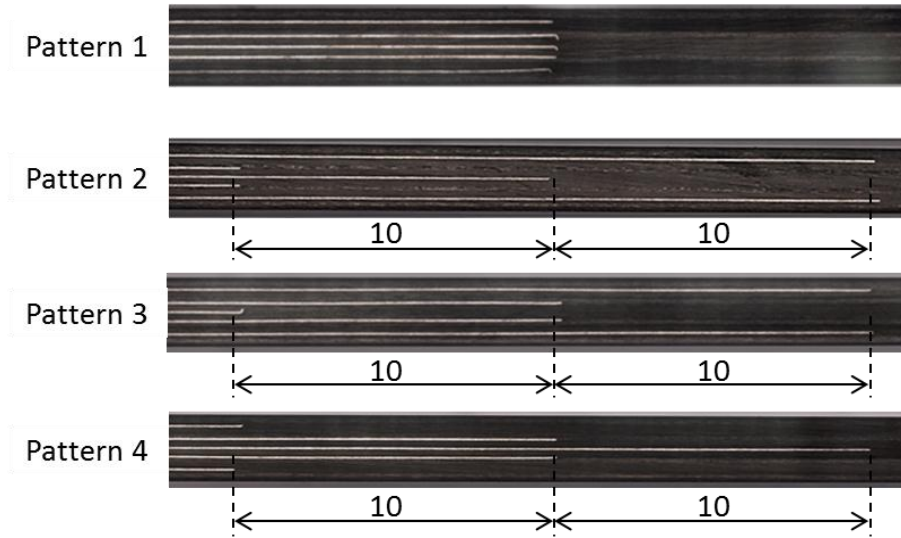


Fig.16 Four different patterns of the transition region

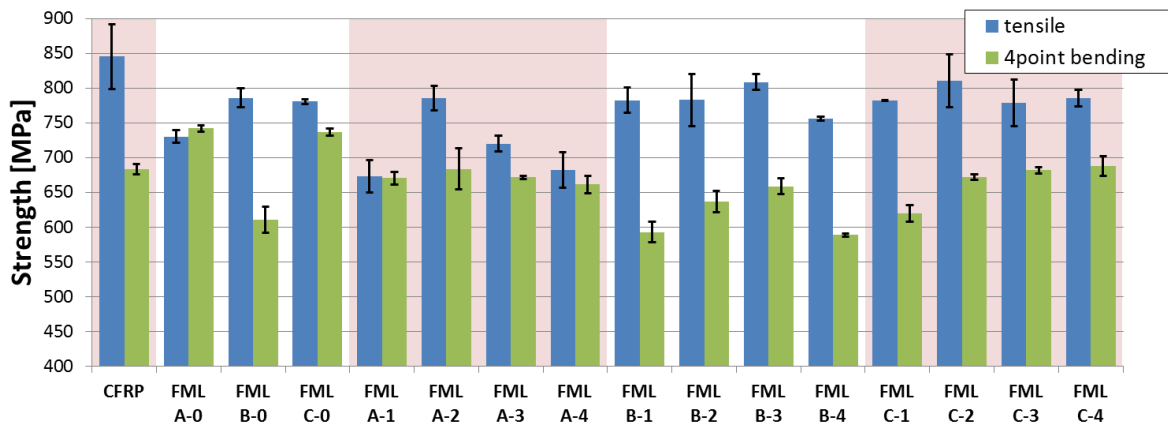


Fig. 17 Tensile and bending strength

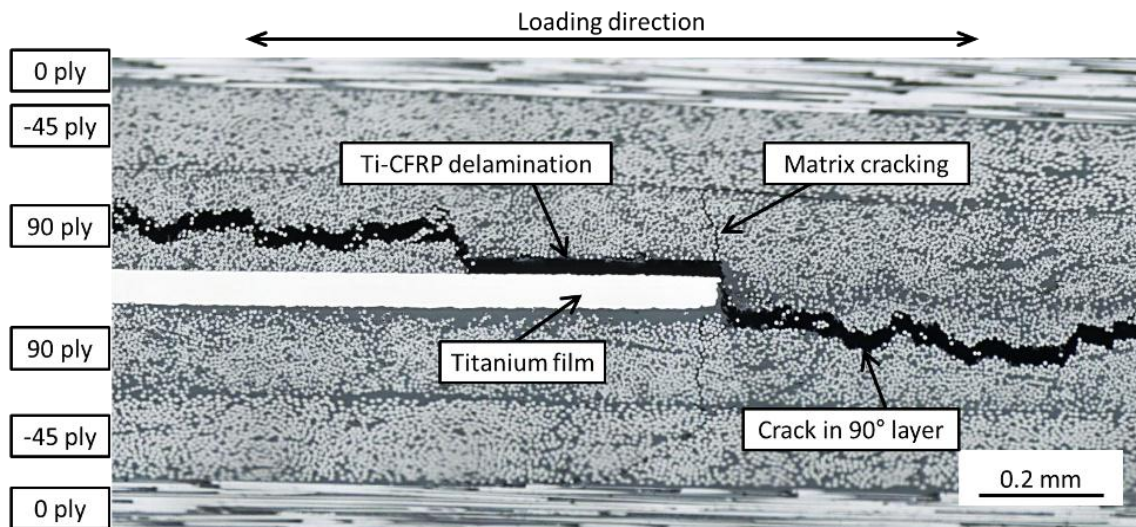


Fig. 18 Damages in 90° layer near the titanium film edge of FML-C-2 under stress of 730MPa

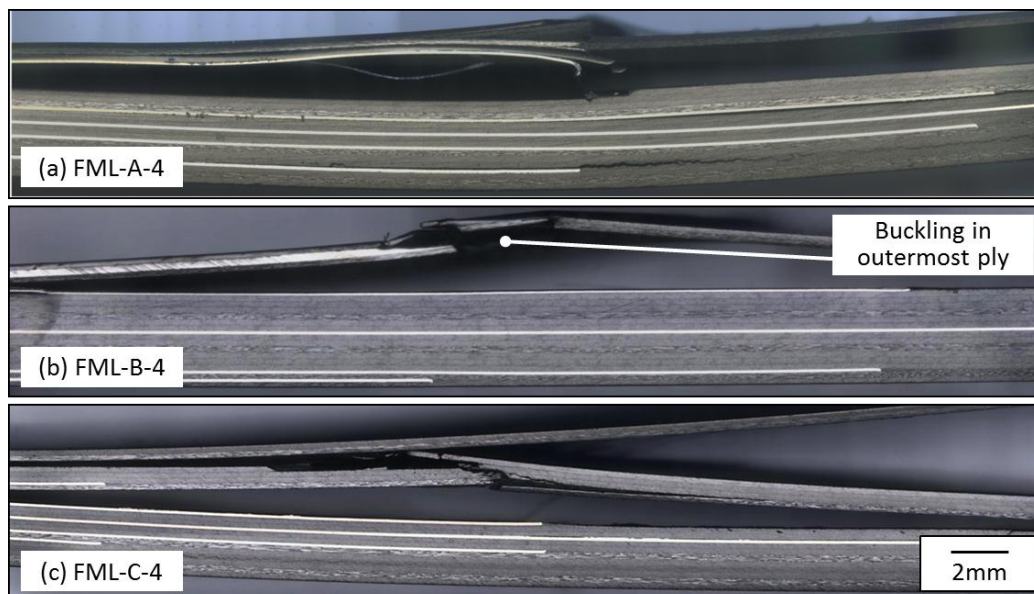


Fig. 19 Damage aspects of the hybrid laminates after bending fracture

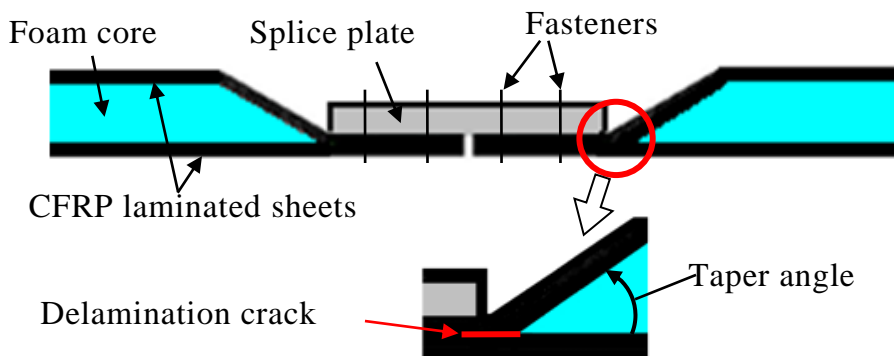


Fig. 20 Configurations of a tapered end-closure type joint

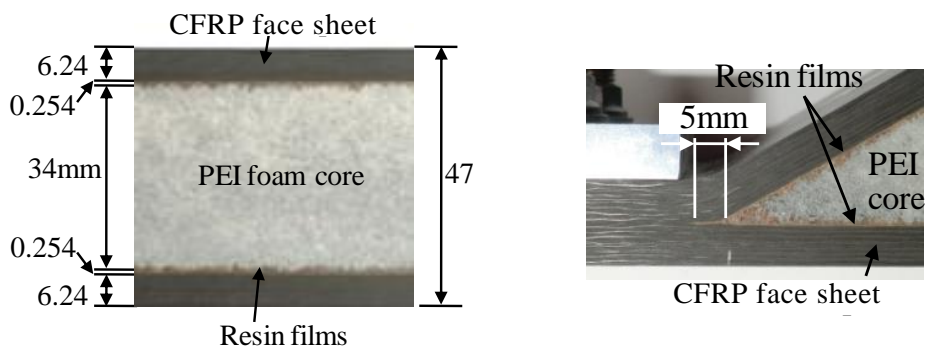


Fig. 21 Dimensions of the test piece

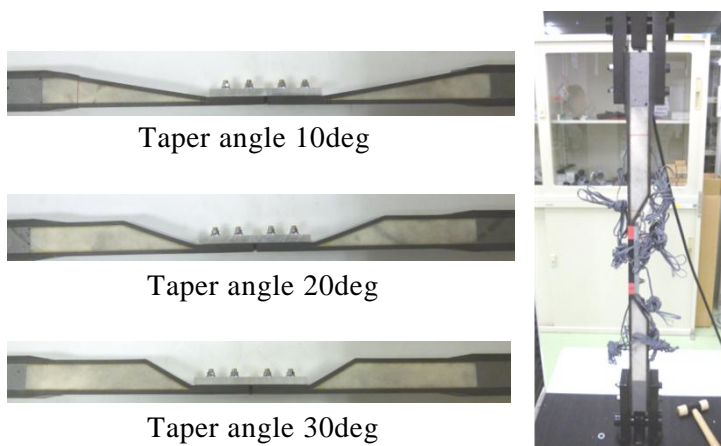


Fig. 22 Photographs of the test pieces

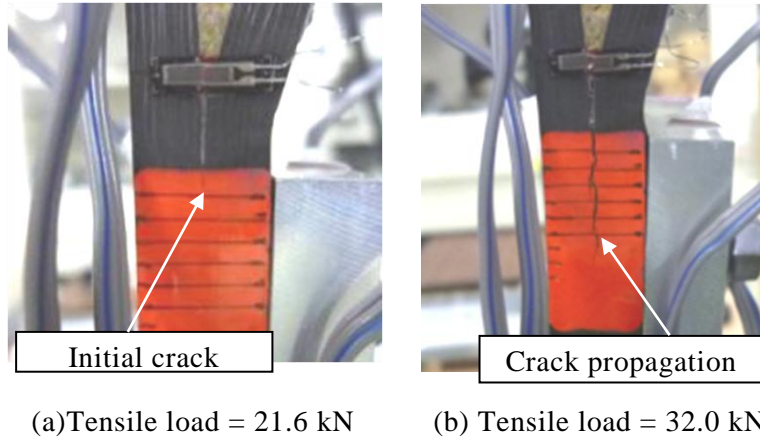


Fig. 23 Photographs of a delamination crack

Table 3 Initial failure load

Taper angle [deg]	Initial failure load [kN]		
10	-1	28.20	ave. 28.0
	-2	27.37	
	-3	28.50	
20	-1	21.60	ave. 21.6
	-2	21.60	
	-3	21.60	
30	-1	17.05	ave. 17.6
	-2	18.05	
	-3	17.70	

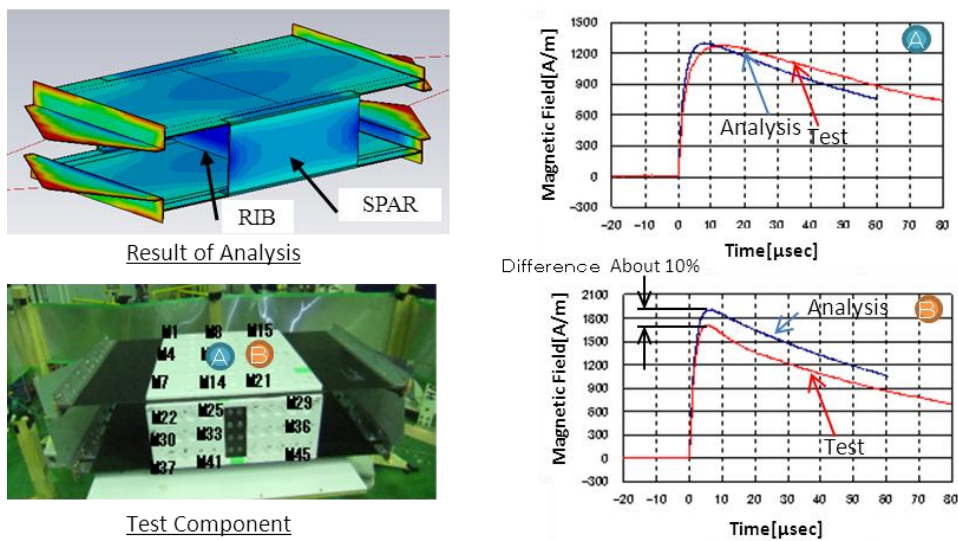
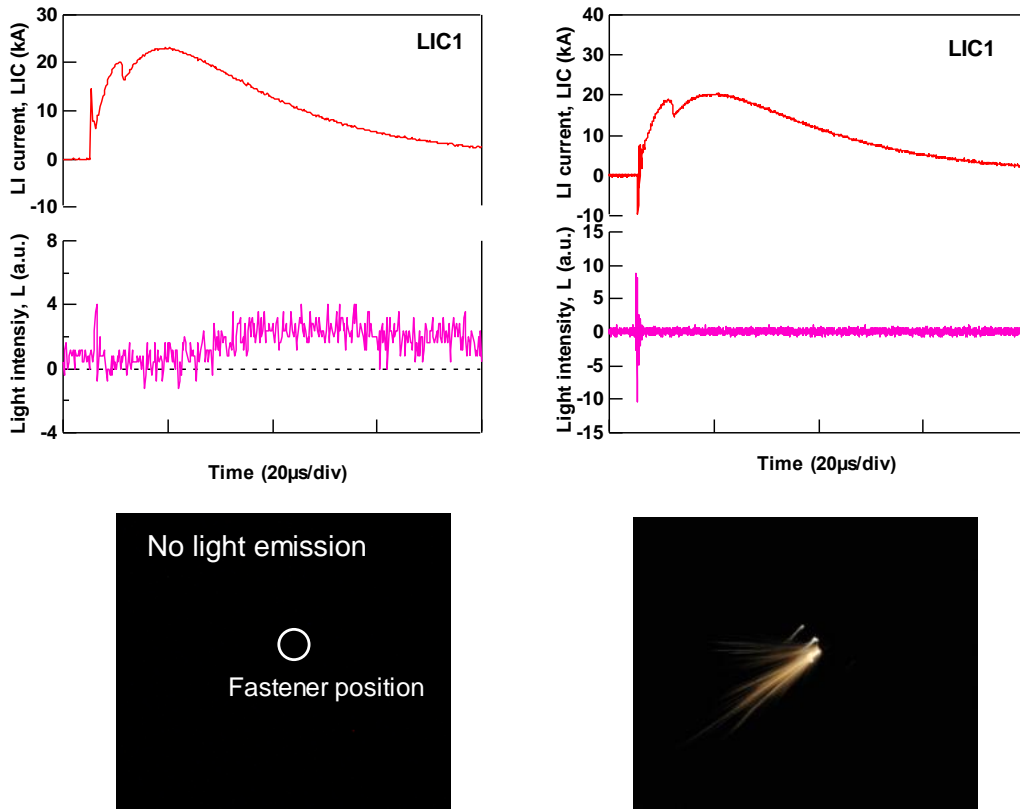


Fig. 24 Example of analysis vs. test result



(a) $I_p = 20.4$ kA (LIC1)

(b) $I_p = 23.1$ kA (LIC1)

Fig. 25 Example of test results

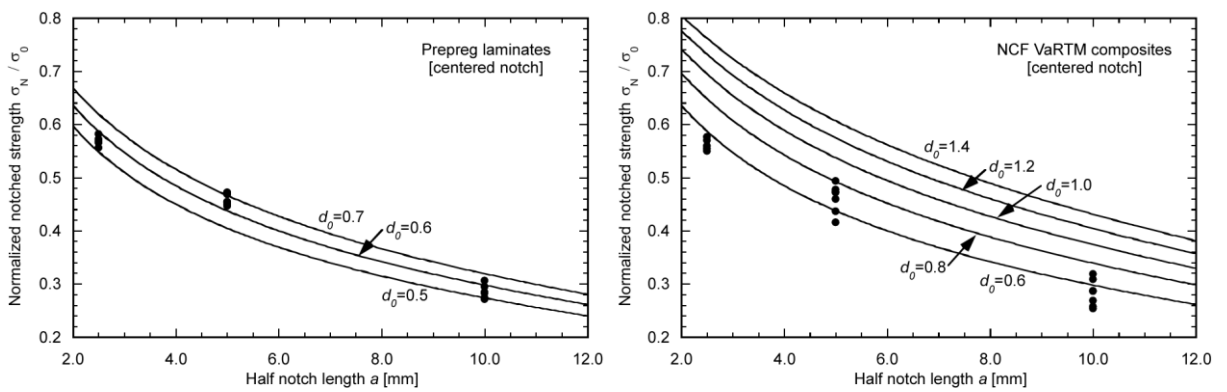


Fig. 26 Notched strength prediction by PSC for the prepreg laminates and the NCF based composites

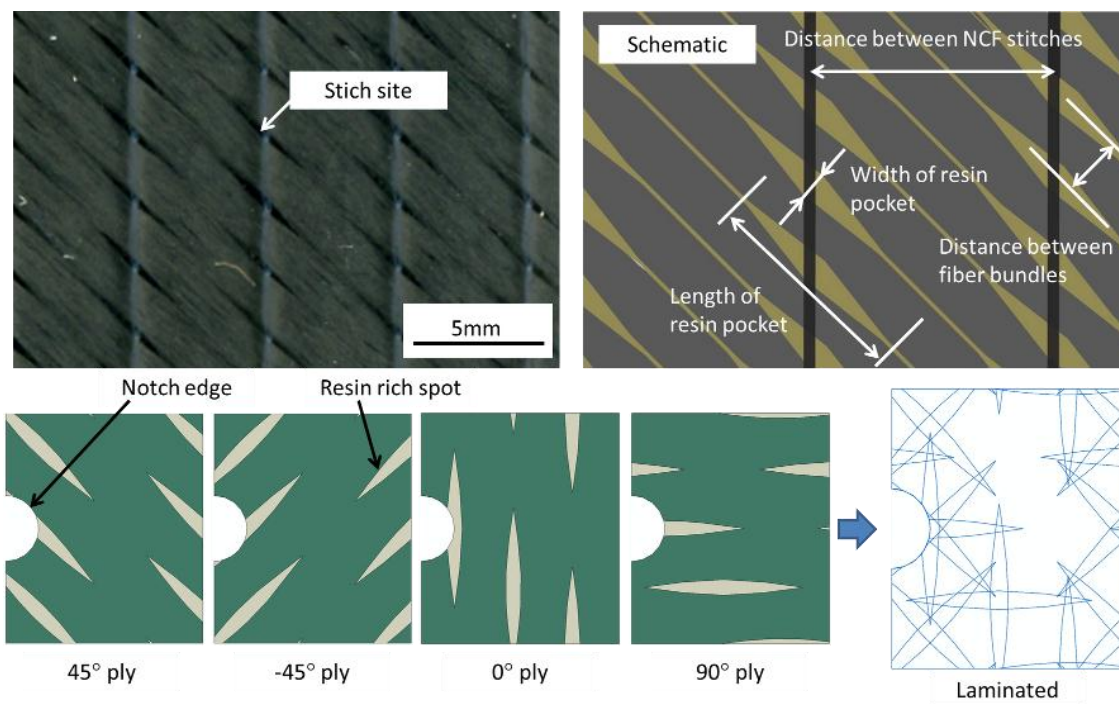


Fig. 27 Resin pockets around stitch sites and FE modeling of NCF based composites

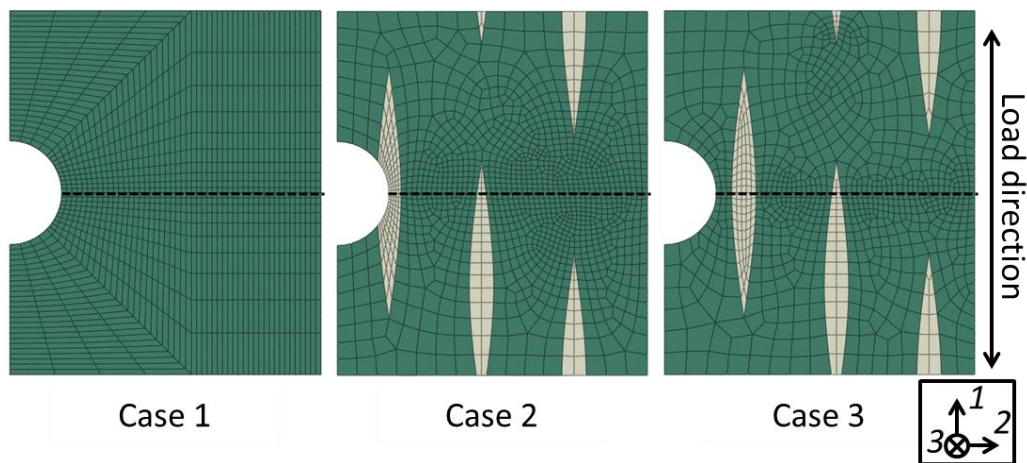


Fig. 28 Schematic of the FE models for 0° ply in the NCF based composites

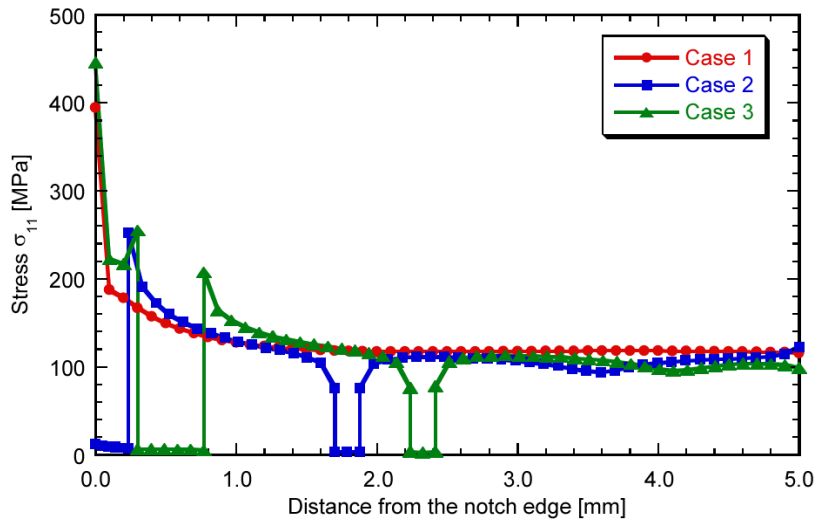


Fig. 29 Stress in fiber direction as a function of the distance from the notch edge.

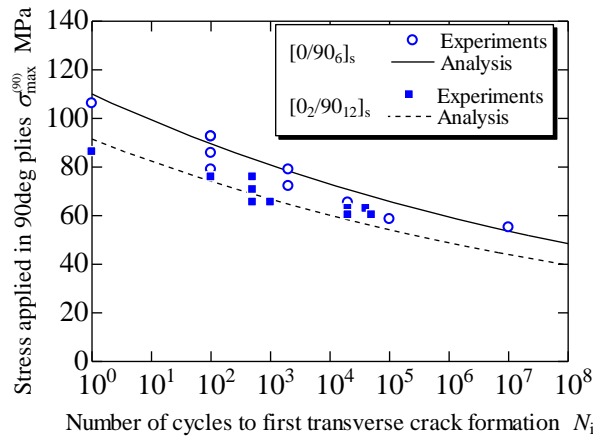


Fig. 30 Prediction of first transverse crack formation under fatigue loading of $[0/90_6]_s$ and $[0_2/90_{12}]_s$ laminates with $V_f=68\%$.

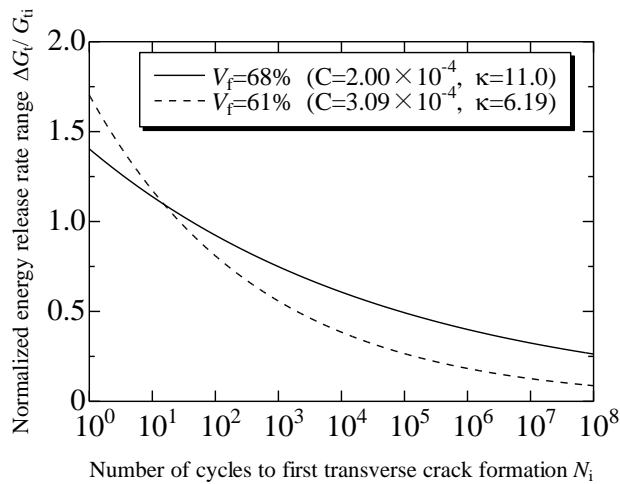


Fig. 31 Comparison of fatigue life for the first transverse crack formation on fiber volume fraction

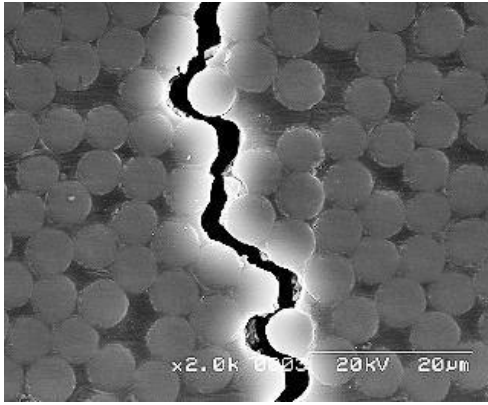


Fig. 32 Fracture pattern of transverse cracking under fatigue loading.

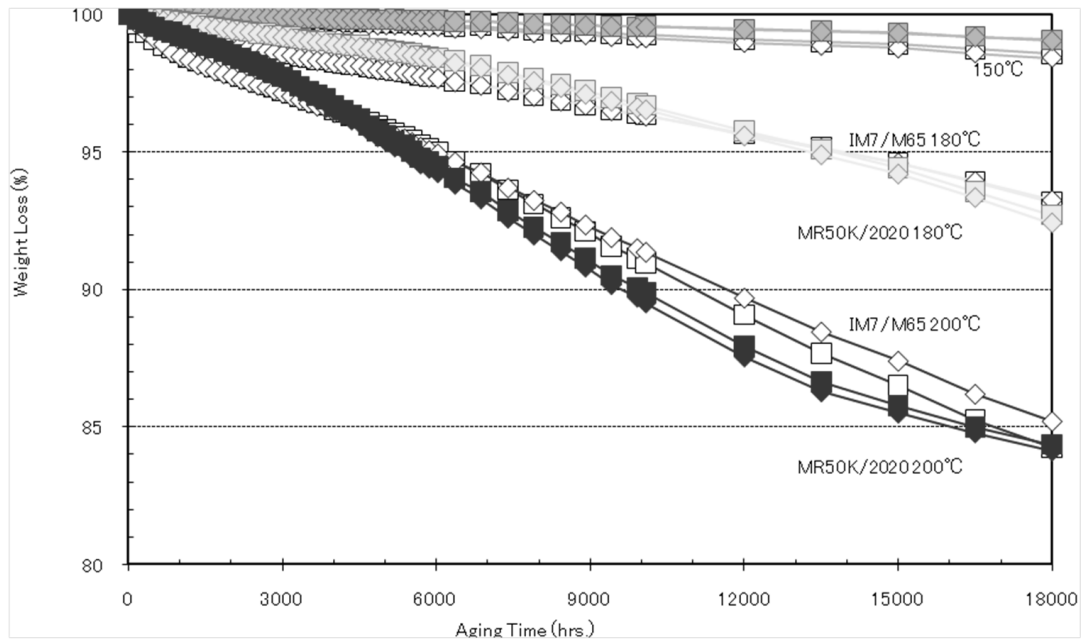


Fig. 33 Weight loss during aging

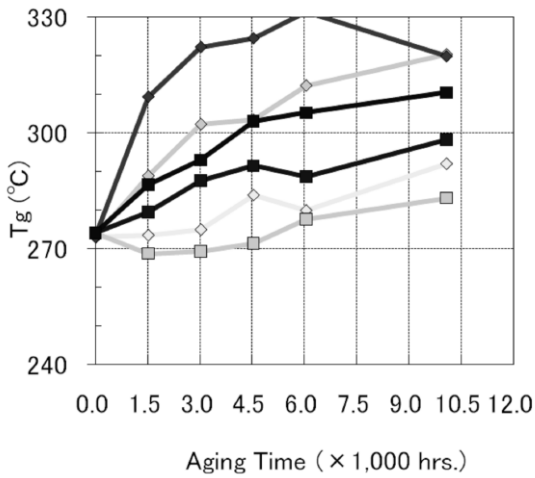


Fig. 34 T_g evolution after aging

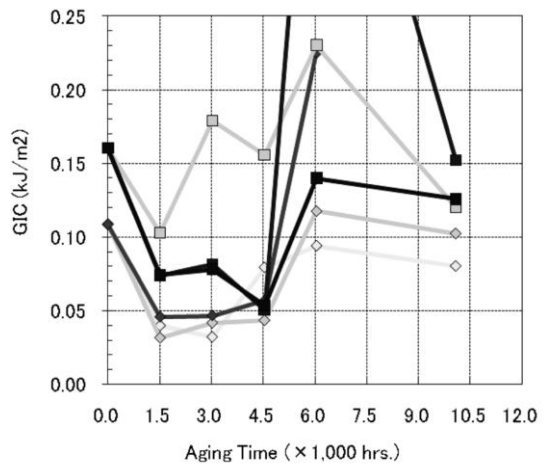


Fig. 35 G_{Ic} evolution after isothermal aging

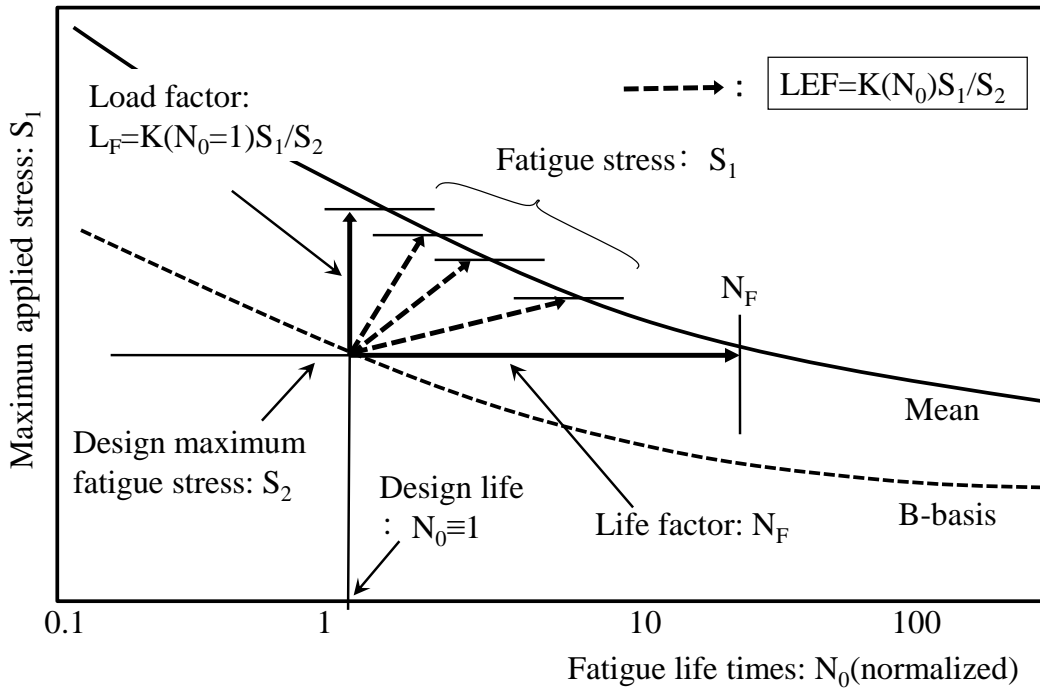


Fig.36 Load enhancement factor approach

Conventional LEF approach(CMH-17)

General form of LEF

- Probability distribution of fatigue life L and residual strength r : 2-parameters Weibull distribution, $W(L|\alpha_L, \beta_L)$ and $W(r|\alpha_r, \beta_r)$
- Load enhancement factor

$$LEF = (N_F/N)^{\alpha_L/\alpha_r} \quad (A1)$$
- Modal values of α_L and α_r

Bayesian expected value of LEF: \underline{LEF}

- Statistical model for shape parameters : Log-normal distributions, $LN(\alpha_L|\mu_L, \sigma_L^2)$ and $LN(\alpha_r|\mu_r, \sigma_r^2)$
- Posterior distributions, $h(\mu_L, \sigma_L^2)$ and $h(\mu_r, \sigma_r^2)$ based on Bayesian conjugate analysis

- Marginal distributions for α_L and α_r

$$f(\alpha) = \iint LN(\alpha|\mu, \sigma^2) h(\mu, \sigma^2) d\mu d\sigma^2 \Big|_{L,r} \quad (A2)$$

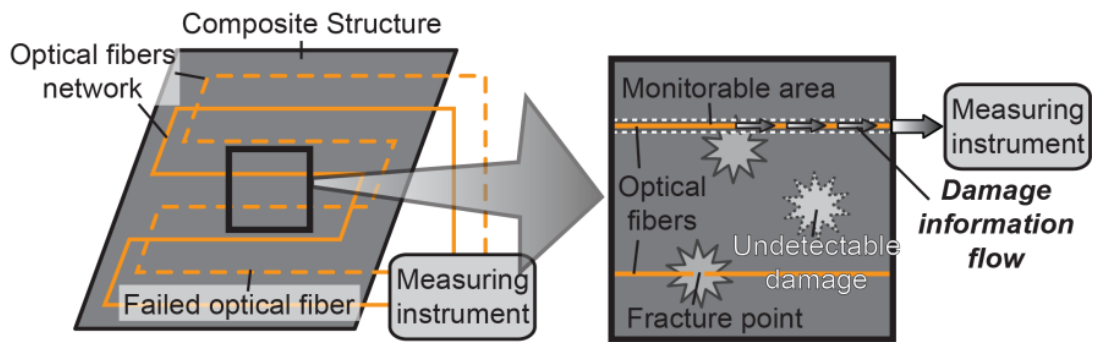
- Bayesian expected value of LEF

$$\underline{LEF} = \iint LEF(\alpha_L, \alpha_r) f(\alpha_L) f(\alpha_r) d\alpha_L d\alpha_r \quad (A3)$$

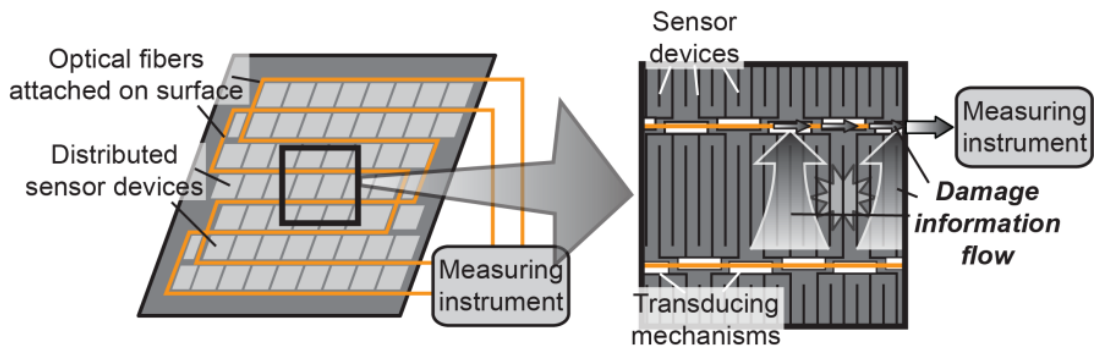
Fig.37 Comparison of LEF approach with Bayesian LEF analysis

Table 4 Expected values of LEF

N ₀	LEF (Bayesian expectation)			LEF(CMH-17)
	Case 1 $\alpha_l < \alpha_r$	Case 2 $\alpha_l < 0.5\alpha_r$	Case 3 $\alpha_l < 0.25\alpha_r$	$\alpha_{L,mode}=1.25$ $\alpha_{r,mode}=20.0$
1	1.35	1.31	1.24	1.18
2	1.23	1.21	1.17	1.13
3	1.17	1.16	1.13	1.10
5	1.11	1.10	1.08	1.06
10	1.03	1.03	1.02	1.02
13.3	1	1	1	1
25	0.94	0.94	0.95	0.961



(a) Existing sensing system utilizing optical fiber network.



(b) Hierarchical sensing system combining distributed sensor devices and optical fibers

Fig. 38 Comparison of sensing system

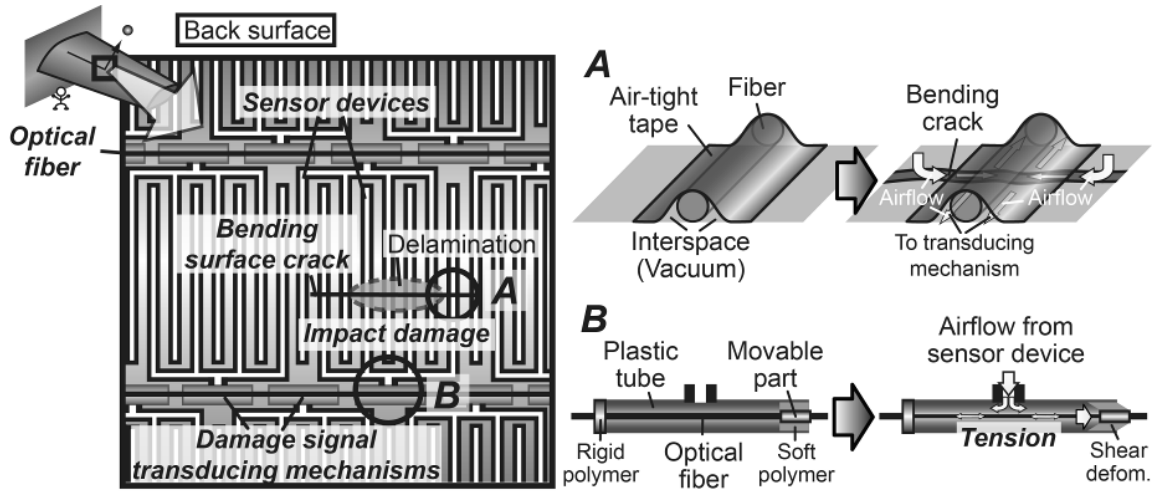
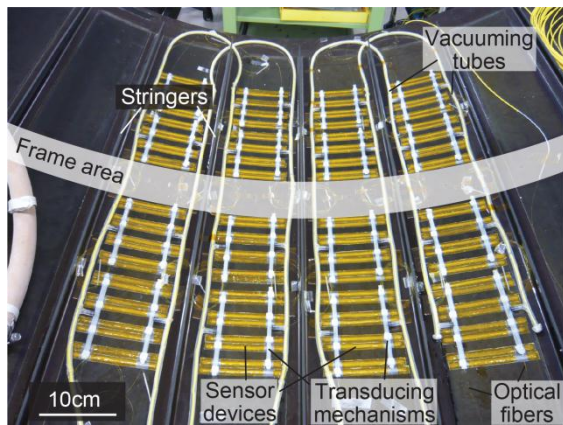
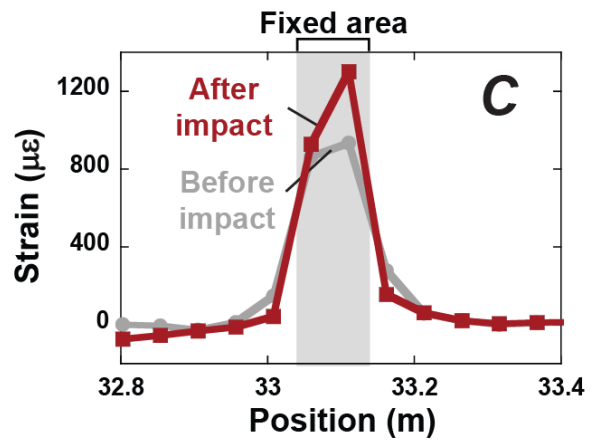


Fig. 39 Hierarchical impact damage detection system



(a) Structural backsurface



(b) Strain increase in damaged area

Fig. 40 Hierarchical surface-crack detection system deployed on CFRP fuselage structure [3]. The hierarchical system has wider monitorable wide, higher robustness and better reparability compared to conventional fiber-optic-based systems.

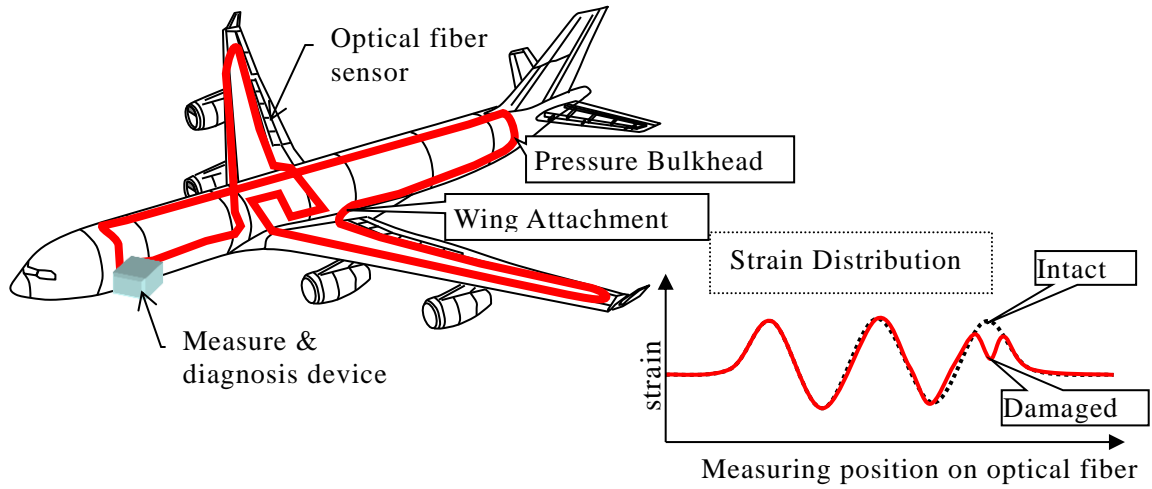


Fig. 41 BOCDA-SHM system application concept

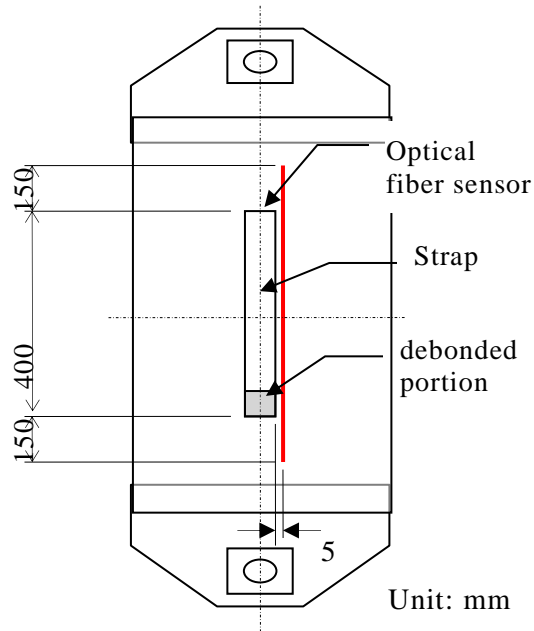
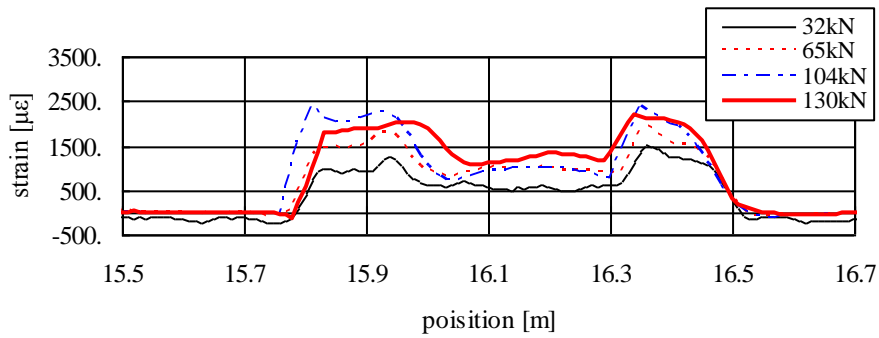


Fig. 42 Test specimen and test stage of debonding damage detection test



T1 30

Fig. 43 Strain distribution in delamination detection tests

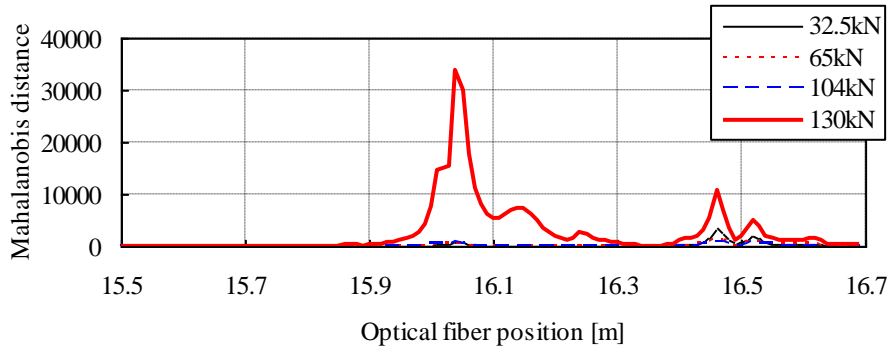


Fig. 44 Delamination diagnosis distribution on the delamination detection tests

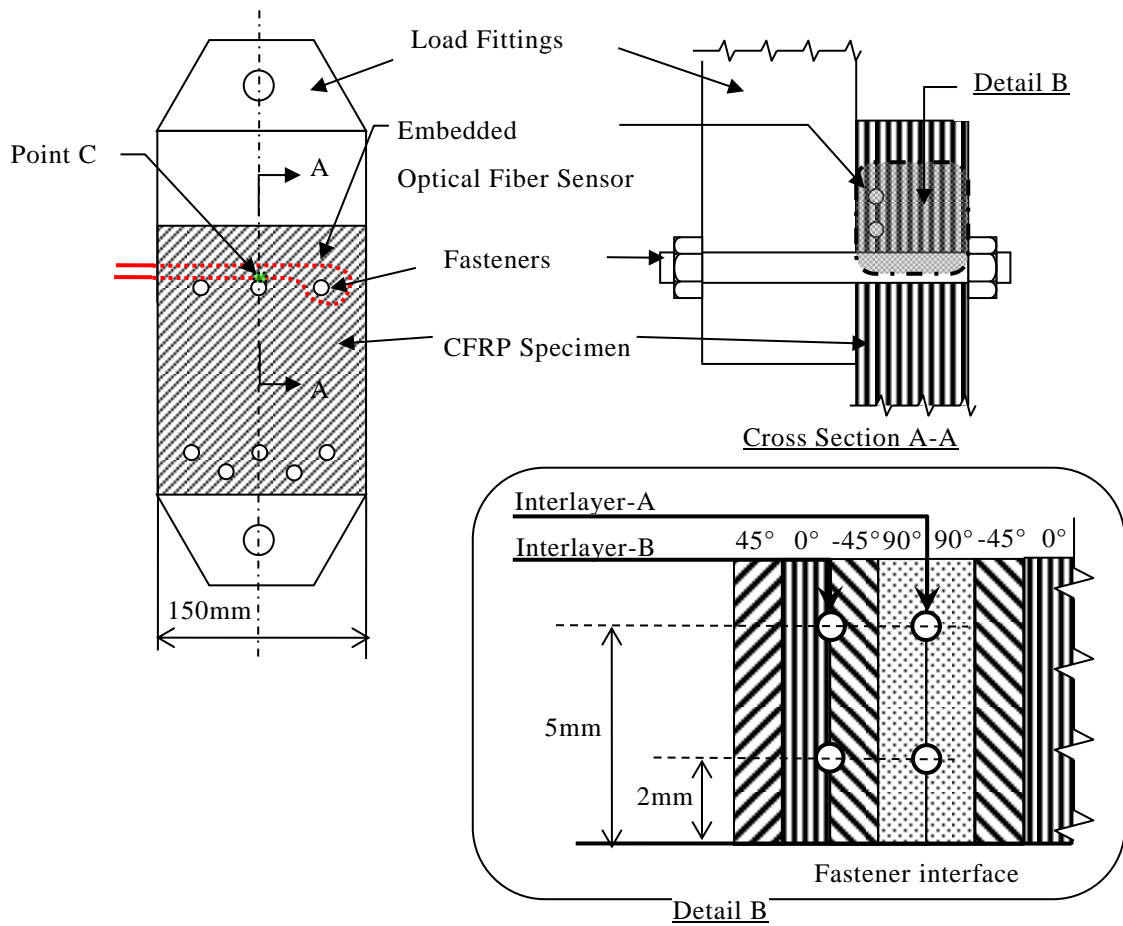


Fig. 45 Test specimen of bearing damage test

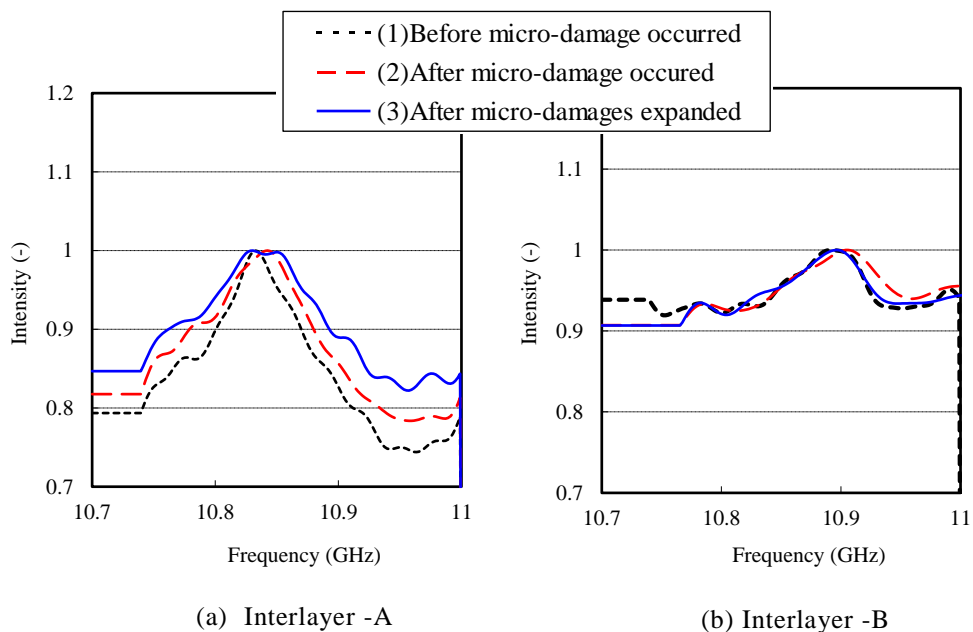


Fig. 46 BGS shapes change at point C. (1) before micro-damages occurred, (2) after micro-damages occurred and (3) after micro-damages expanded.

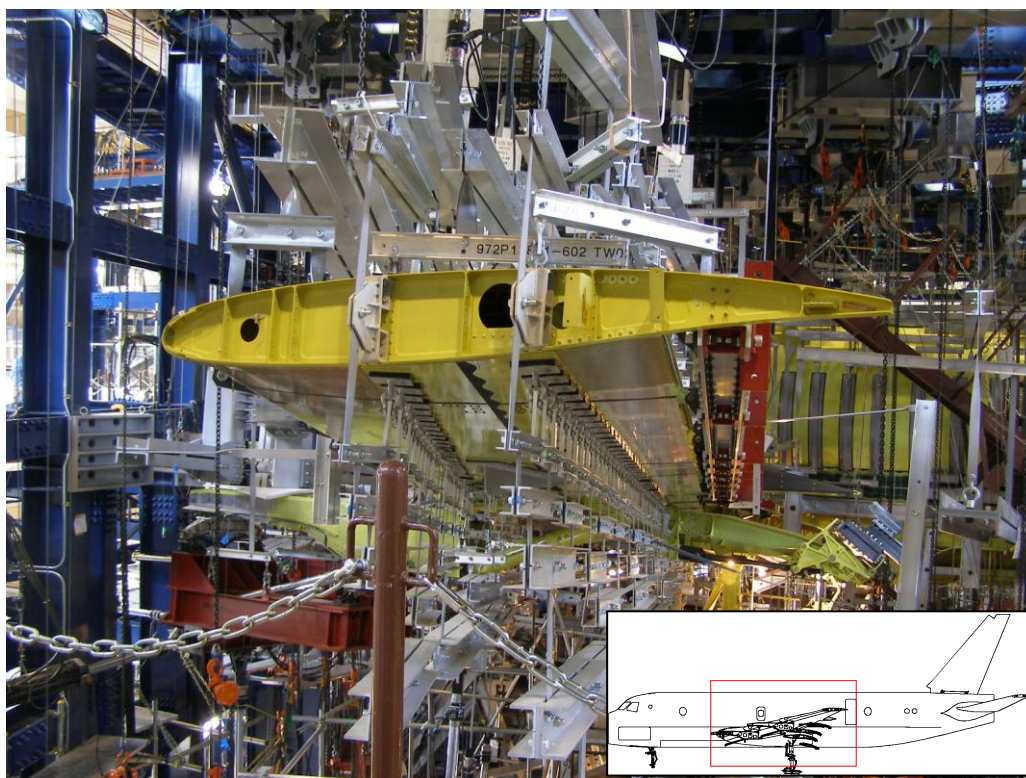


Fig. 47 Full Scale Fatigue Test of XP-1

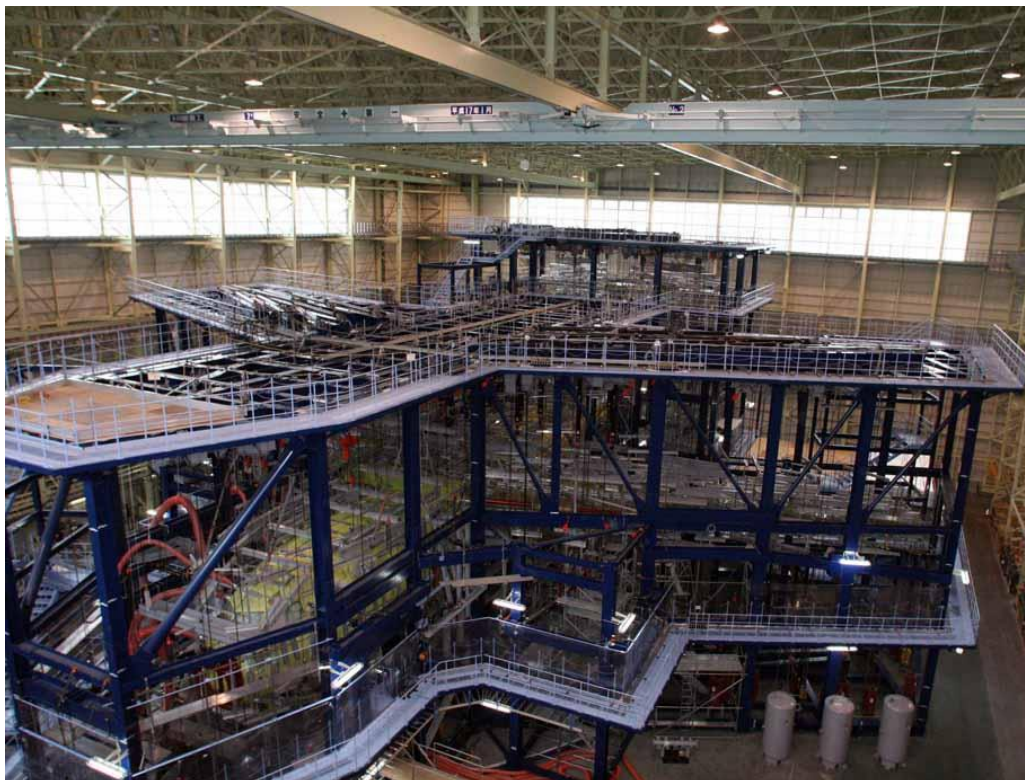


Fig. 48 Full Scale Fatigue Test of XC-2



Fig. 49 Picture of Sabreliner 80 and its original metal speedbrake

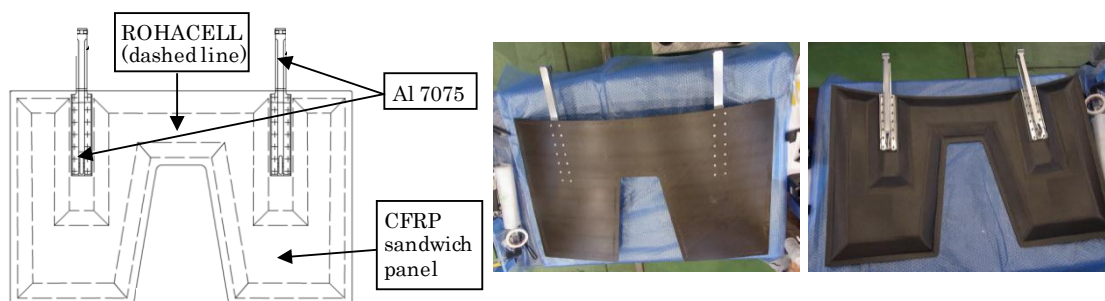


Fig. 50 Manufactured composite speedbrake

Table 5 Used materials for composite speedbrake.

Material	Specification
VaRTM	Fabric; SHINDO U200C-80S (Toray T800SC UD sheet)
	Resin; Nagase ChemteX XNR/HNR2250 (180 deg. C cure)
Prepreg	UMECO T800SC /MTM45-1 (180 degrees C cure)
Core	ROHACELL 71WF
Adhesive	3M scotch - weld AF3109 - 2

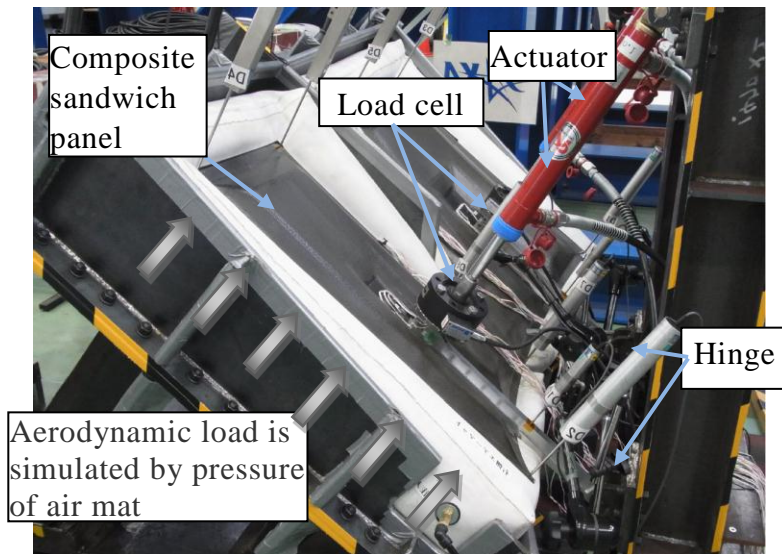


Fig. 51 Structural strength test of a CFRP speedbrake.

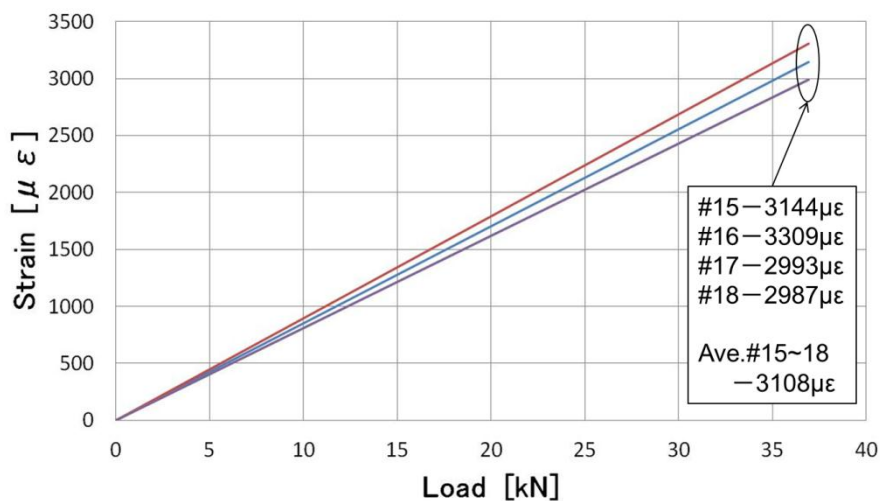


Fig. 52 Ultimate load test result of composite speedbrake at point 15, 16, 17, 18 in Fig. 50.